2017

COMPUTATIONAL INVESTIGATION OF TRANSMURAL DIFFERENCES IN LEFT VENTRICULAR CONTRACTILITY AND HYDROGEL INJECTION TREATMENT FOR MYOCARDIAL INFARCTION

Hua Wang
University of Kentucky, hwa229@g.uky.edu
Digital Object Identifier: https://doi.org/10.13023/ETD.2017.226

STUDENT AGREEMENT:

I represent that my thesis or dissertation and abstract are my original work. Proper attribution has been given to all outside sources. I understand that I am solely responsible for obtaining any needed copyright permissions. I have obtained needed written permission statement(s) from the owner(s) of each third-party copyrighted matter to be included in my work, allowing electronic distribution (if such use is not permitted by the fair use doctrine) which will be submitted to UKnowledge as Additional File.

I hereby grant to The University of Kentucky and its agents the irrevocable, non-exclusive, and royalty-free license to archive and make accessible my work in whole or in part in all forms of media, now or hereafter known. I agree that the document mentioned above may be made available immediately for worldwide access unless an embargo applies.

I retain all other ownership rights to the copyright of my work. I also retain the right to use in future works (such as articles or books) all or part of my work. I understand that I am free to register the copyright to my work.

REVIEW, APPROVAL AND ACCEPTANCE

The document mentioned above has been reviewed and accepted by the student's advisor, on behalf of the advisory committee, and by the Director of Graduate Studies (DGS), on behalf of the program; we verify that this is the final, approved version of the student's thesis including all changes required by the advisory committee. The undersigned agree to abide by the statements above.

<div align="right">

Hua Wang, Student

Dr. Jonathan F. Wenk, Major Professor

Dr. Haluk Karaca, Director of Graduate Studies

</div>

COMPUTATIONAL INVESTIGATION OF TRANSMURAL DIFFERENCES IN
LEFT VENTRICULAR CONTRACTILITY AND HYDROGEL INJECTION
TREATMENT FOR MYOCARDIAL INFARCTION

_____

DISSERTATION
_____

A dissertation submitted in partial fulfillment of the
requirements for the degree of Doctor of Philosophy in the
College of Engineering
at the University of Kentucky

By

Hua Wang

Lexington, Kentucky

Co-Director: Dr. Jonathan F. Wenk, Professor of Mechanical Engineering
and   Dr. Keith E. Rouch, Professor of Mechanical Engineering

Lexington, Kentucky

2017

ABSTRACT OF DISSERTATION

COMPUTATIONAL INVESTIGATION OF TRANSMURAL DIFFERENCES IN
LEFT VENTRICULAR CONTRACTILITY AND HYDROGEL INJECTION
TREATMENT FOR MYOCARDIAL INFARCTION

Heart failure (HF) is one of the leading causes of death and impacts millions of people throughout the world. Recently, injectable hydrogels have been developed as a potential new therapy to treat myocardium infarction (MI). This dissertation is focused on two main topics: 1) to gain a better understanding the transmural contractility in the healthy left ventricle (LV) wall and 2) investigate the efficacy of the hydrogel injection treatment on LV wall stress and function. The results indicate that a non-uniform distribution of myocardial contractility in the LV wall provide a better representation of normal LV function. The other important study explored the influence altering the stiffness of the biomaterial hydrogel injections. These results show that a larger volume and higher stiffness injection reduce myofiber stress the most and maintaining the wall thickness during loading. The computational approach developed in this dissertation could be used in the future to evaluate the optimal properties of the hydrogel. The last study used a combination of MRI, catheterization, finite element (FE) modeling to investigate the effects of hydrogel injection on borderzone (BZ) contractility after MI. The results indicate that the treatment with hydrogel injection significantly improved BZ function and reduce LV remodeling, via altered MI properties. Additionally, the wall thickness in the infarct and BZ regions were significantly higher in the treated case. Conclusion: hydrogel injection could be a valuable clinical therapy for treating MI.

KEYWORDS: Finite element modeling, Hydrogel injection, Myocardial infarction, Computational optimization

Hua Wang
Student's Signature

04/14/2017
Date

COMPUTATIONAL INVESTIGATION OF TRANSMURAL DIFFERENCES IN
LEFT VENTRICULAR CONTRACTILITY AND HYDROGEL INJECTION
TREATMENT FOR MYOCARDIAL INFARCTION

By

Hua Wang

<div align="right">

Dr. Jonathan F. Wenk
Co-Director of Dissertation

Dr. Keith E. Rouch
Co-Director of Dissertation

Dr. Haluk Karaca
Director of Graduate Studies

04/14/2017
Date

</div>

To my family

ACKNOWLEDGEMENTS

It would not have been possible to write this dissertation without the help and support of the kind people around me.

Foremost, I would like to express my sincere gratitude to my graduate advisor Prof. Jonathan Wenk, for his excellent guidance, patience and providing me with an excellent atmosphere for doing research, for enlightening me the first glance of research. Special thanks goes to Prof. Keith Rouch, Prof. Haluk Karaca, Prof. Kenneth Campbell and Prof. Peter Kekenes-Huskey who were willing to participate in my final doctoral defense committee.

Besides, I would like to thank my labmates in Computational Biomechanics Laboratory (CBL): Dimitri Mojsejenko, Xiaoyan Zhang, Amir Nikou, Zhanqiu Liu and Dara Sigh for the stimulating discussions and all the fun we have had in the last five years.

Finally, I would like to thank my parents and my husband, they were always supporting me and encouraging me with their best wishes, also cheering me up and stood by me through the good times and bad.

TABLE OF CONTENTS

LIST OF TABLES

LIST OF FIGURES

Chapter 1   **INTRODUCTION**

1.1   Motiviation

Cardiovascular disease remains a leading cause of morbidity and mortality worldwide. According to the 2016 American Heart Association Statistics, more than 17.3 million people die each year and is number is projected to increase to more than 23.6 million by 2030 [1]. Several mechanisms that lead to systolic heart failure (HF) include atherosclerosis, hypertension, myocardial infarction and mitral regurgitation. This dissertation is focused on the effects of myocardial infarction. According to the report statistic, roughly 785,000 people in the United States have a myocardial infarction each year, which can eventually lead to chronic heart failure [1]. An estimated 82.6 million American adults (>1 in 3) have 1 or more types of cardiovascular disease. In the state of Kentucky, more than 40% of adults have multiple risk factors. In terms of economic impact, the total cost due to cardiovascular disease exceeded $286 billion.

Since heart failure is a significant medical burden to the developed world, there is a need for better solutions to solve this problem. In order to address the issue of myocardial infarction, biomaterial injections have recently been proposed as a potential new therapy for augmenting ventricular mechanics after myocardial infarction. This approach could reduce the stress in the failing ventricular wall and act to retard the progression of heart failure. In order to better understand the mechanical effects of this treatment, new methods that combine magnetic resonance imaging (MRI), catheterization and finite element (FE) modeling are

being used to investigate hearts that are healthy, diseased and/or treated. This method could be used to observe how the stress changed in the ventricular wall. Since myocardial contractility of the left ventricle wall plays an essential role in maintaining normal pump function, it is important to have proper parameters to describe left ventricular behavior when analyzing contractility with numerical simulation. Additionally, the efficacy of using biomaterial injections, which could be used to treat myocardial infarction, has motivated the use of computational methods to investigate the stress reduction in different regions after myocardial infarction.

1.2   Background on structure and function

The heart is an integral part of the cardiovascular system and is composed of four primary chambers: right atrium, right ventricle, left atrium and left ventricle. The left ventricle (LV) is the strongest chamber among these four chambers and pumps oxygen-rich blood to the rest the body. This dissertation is focusing on the LV as it can be significantly affected by cardiovascular disease. The left ventricular wall consists of three layers, epicardium, myocardium and endocardium. Myocardial contractility depends on several factors, including action potential morphology, Ca^+ dynamics, and sarcomere length (Figure 1) [2]. It has been shown in previous studies that these factors vary as a function of transmural location in the LV wall [3, 4]. Also, some ex-vivo experimental studies have examined the difference in isometric force generation in permeabilized cardiomyocytes, but only in samples from the sub-epicardium and sub-

2

endocardium of the LV [5, 6]. However, a recent study examined cardiomyocyte samples from all three transmural regions and showed that maximum isometric force generation exhibits transmural heterogeneity in healthy human hearts with the mid-myocardium generating greater force than the sub-endocardium and sub-epicardium [7]. However, there is no computational results which report that myocardial force generation varies transmurally. Better understanding the contractility in the LV wall will be explained in chapter 3.

The distribution of stress in the LV wall is impacted by both the fiber tension and fiber orientation. In 1969, the paper by Streeter et al. [8] indicated that the myocardial wall has a well-ordered distribution of fiber angle ranged from -60° to 60° (from epicardium to endocardium) in normal canine heart. Besides this, in comparison to normal heart, the fiber angles changed in pressure-overload heart. As mentioned in Carew et al. [9], the fiber angle was tested between -67.5° and -90° in endocardium and ranged from 67.5° to 90° in epicardium. The method used to study the fiber orientations was described in the paper [8, 9].

The normal healthy left ventricle has a thick muscular wall, which is shown in Figure 2(A). The healthy heart pumps blood through the network of arteries and veins, which is important for maintaining normal bodily function. However, after myocardial infarction (MI), a coronary artery is suddenly blocked, and cardiac tissue in the LV wall is deprived of oxygen and part of the heart muscle dies. Over time this can lead to ischemia and arrhythmias, which cause a severe decrease in the pumping function of the heart. Figure 2 shows the tissue structure changes after myocardial infarction. Eventually, during remodeling, due to an overload

blood flow and pressure in LV, the LV wall can overstretch and become thinner (Figure 2(B) and Figure 2(C)).

The pathology of MI can be considered as four phases: acute ischemia, the necrotic phase, the fibrotic phase and the remodeling phase. In the first few hours, this is called acute ischemia. It occurs just after infarction; the myocardium loses the ability to generate systolic force [10]. Then the ischemic myocardium behaves as a passive elastic material during the whole cardiac cycle. [10]. The first phase was also described in 1978 by Hutchins and Bulkley, has been termed "infarct expansion" and defined as "acute dilatation and thinning of the area of infarction not explained by additional myocardial necrosis" [11]. As a result in this phase, the mechanics of the infarcted myocardium changed from active material to passive material [10]. The second phase is called necrotic phase, and usually lasts about 7 days in human and 5 days in rat [12]. The stiffness of the infarct region was increased during this phase [10]. There are two changes in mechanics in this phase. First is that, the stiffness in circumferential and longitudinal direction is increased under multiaxial loading but there is no apparent change in uniaxial loading [10]. The second is that, at least in circumferential direction, unstressed segment length increases whereas end-diastolic length not [10]. The third phase is fibrotic phase. The stiffness of the infarct region is increased and the left ventricle cannot be expand fully due to the malfunction of diastolic filling, which limit the pump function of the heart [10]. During the fourth phase, which is called remodeling phase, the stiffness of infarct tissue is decreased while the stiffness in circumferential direction remains nearly twice that of the longitudinal direction.

The myocardial infarction may affect the infarcted regions and non-infarcted regions. The remodeling process will influence the function of the left ventricle and prognosis for survival. Early infarct expansion or stretching has been associated with poor long-term prognosis [13-15] and has been identified as the mechanical phenomenon that initiates and sustains the process of adverse post-MI LV remodeling that leads to heart failure [16-21]. Infarct expansion causes abnormal stress distribution in myocardial regions within and outside the MI, especially in the adjacent normally perfused borderzone (BZ) region. With time, increased regional stress is the stimulus for maladaptive biologic processes, such as matrix metalloproteinase activation, that inherently alter the contractile properties of normally perfused myocardium [22]. Once initiated, these maladaptive processes lead to a heart failure phenotype that is difficult to reverse by medical or surgical means. Observing the contractility in borderzone region, infarct region and remote region is a way to better understand the remodeling process so that treatment can be improved after MI. LV remodeling is a pathological adaptive process due to myocardial infarction (Figure 3). After the initial insult, infarct expansion and ventricular wall thinning, it contributes to further ventricular remodeling. During the ventricular remodeling process, pressure and radius increase in the LV, and LV free wall thins (Figure 4). This process will increase the cardiac wall stress.

1.3   Overview

The overall goal of this dissertation work is to generate a better FE model of the LV. This was done by investigating normal myocardial function and then

examining the effects of biomaterial injections as a treatment for altering MI mechanics. This work was accomplished using a combination of finite element (FE) modeling, magnetic resonance imaging (MRI) and ventricular pressure catheterization to assess in vivo myocardial material properties in the LV using numerical optimization.

Chapter 2 outlines the constitutive behavior of myocardium (in passive response and active contraction) and hydrogel injections. Chapter 3 is to estimate the in-vivo contractile forces generated in the sub-endocardial, mid-myocardial, and sub-epicardial regions of healthy porcine ventricles. This work was motivated by recent ex-vivo transmural measurements [7]. In Chapter 4 and Chapter 5, I will focus on a therapy using injectable biomaterials to attenuate left ventricular remodeling after myocardial infarction. Specifically, Chapter 4 discusses a numerical sensitivity study of hydrogel injection motived by work done using two different hydrogels to treat myocardial infarction. Chapter 5 investigates the effects of hydrogel injection on borderzone contractility after myocardial infarction. The relevant literature review is detailed in each Chapter.
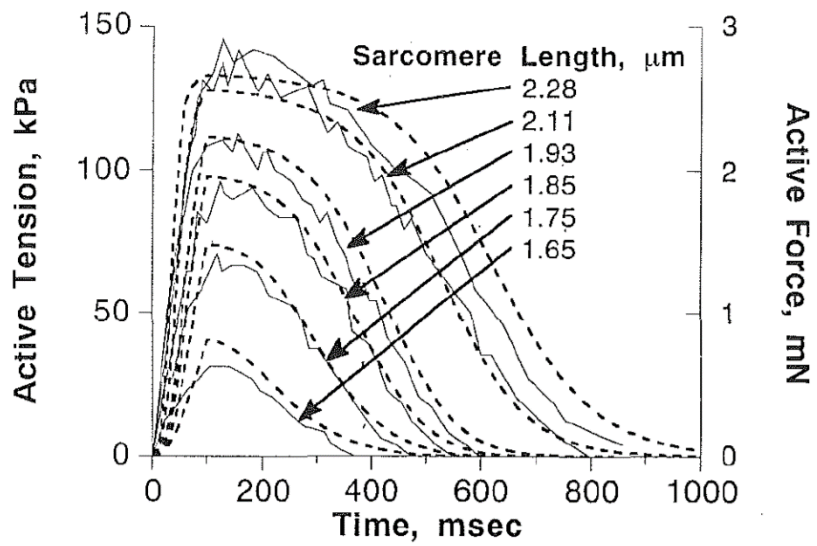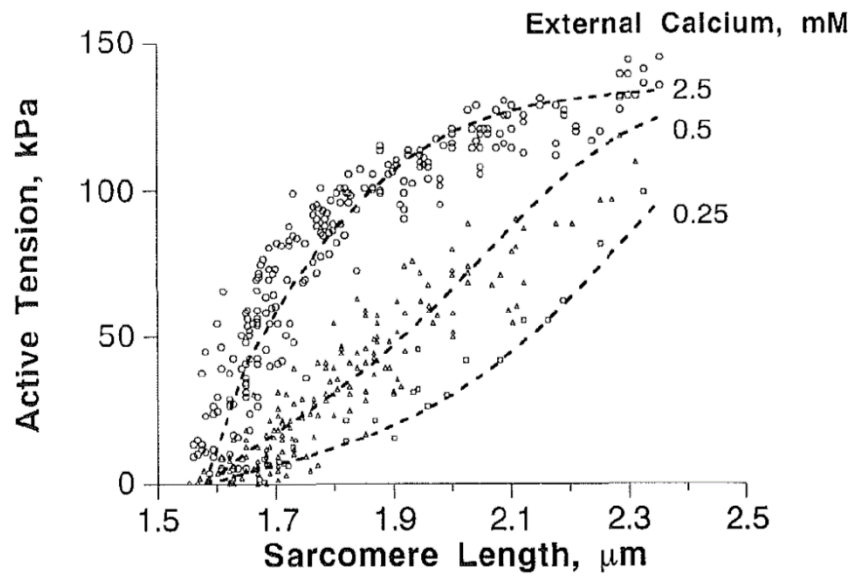
Figure 1 Myofiber systolic contraction depends on calcium concentration (A) and sarcomere length (B) [2] .
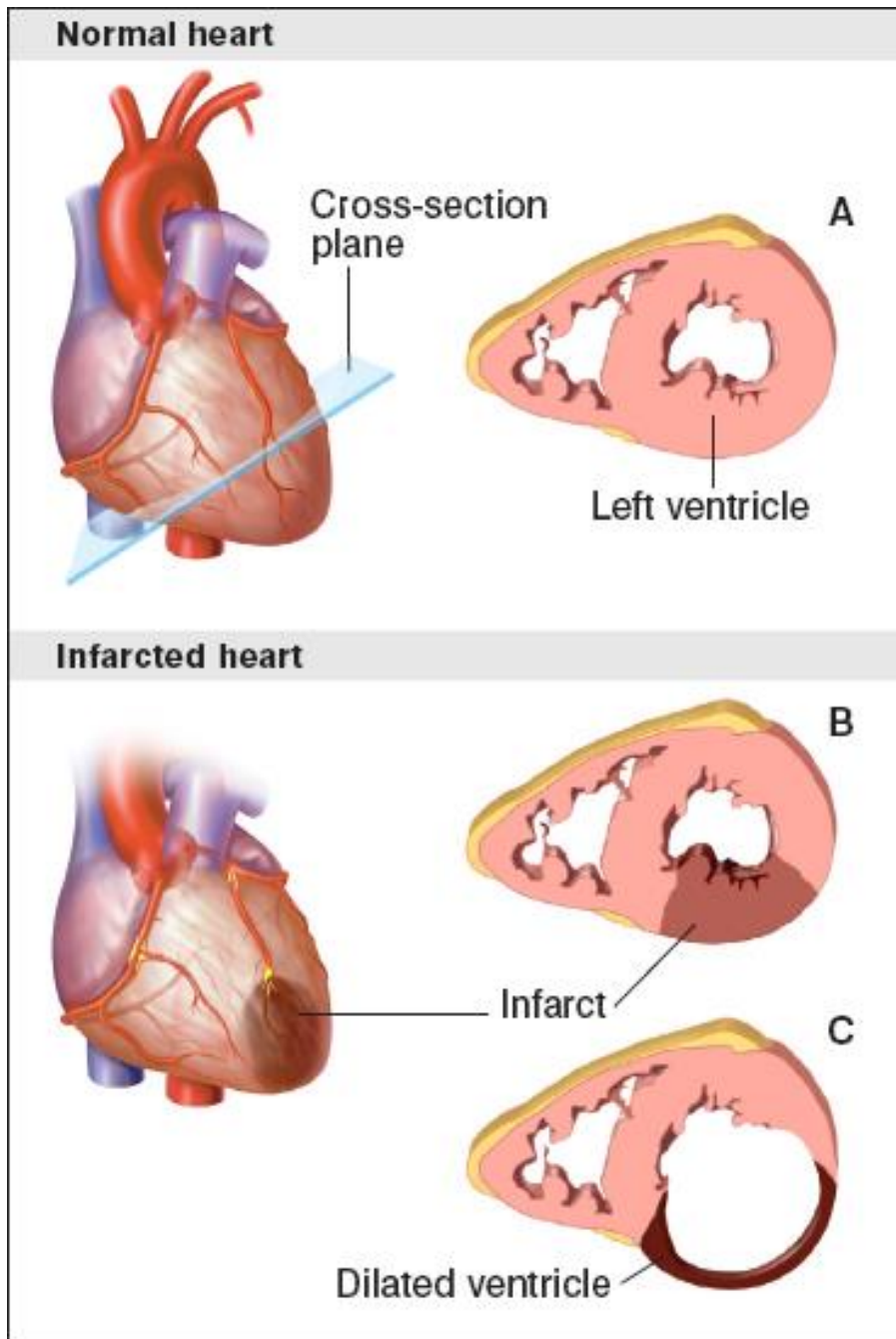
Figure 2 A normal left ventricle wall. B left ventricle wall after myocardial infarction. C Finally causing the ventricle wall to become thinner [23].

Figure 3 Myocardial Wall thickness for normal tissue (remote region) and MI tissue [24].
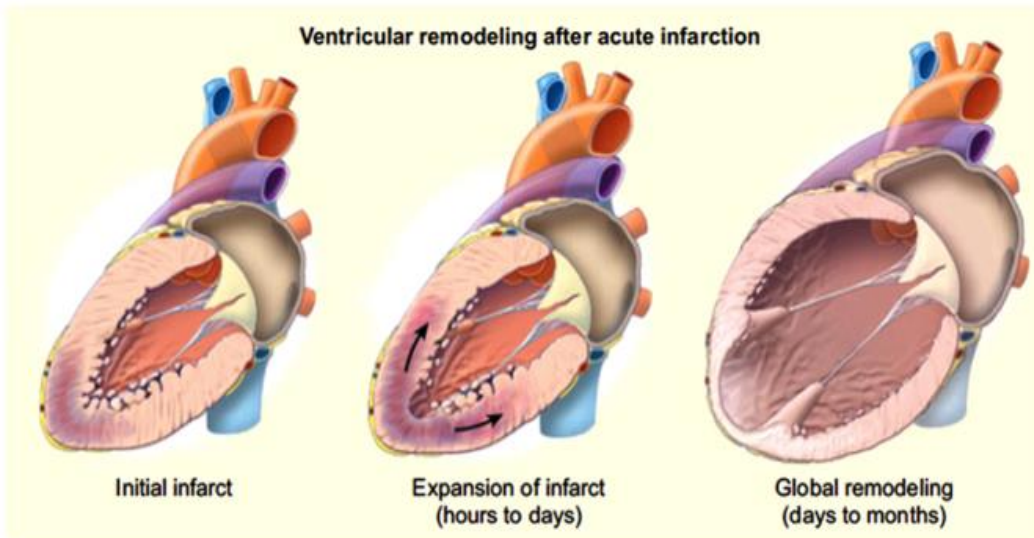
Figure 4 Ventricular remodeling after acute infarction [1].

Chapter 2   **Constitutive behavior**

The material response of the myocardium was represented using a nearly incompressible, transversely isotopic, hyperelastic constitutive law, which was defined using the following strain energy function:

$$W_{myocardium} = \frac{C}{2}\left(e^{b_f E_{ff}^2 + b_t\left(E_{ss}^2 + E_{nn}^2 + E_{ns}^2 + E_{sn}^2\right) + b_{fs}\left(E_{fs}^2 + E_{sf}^2 + E_{fn}^2 + E_{nf}^2\right)} - 1\right) + \frac{\kappa}{2}(J-1)^2$$

(Eq. 1)

where E_{ij} are the deviatoric components of the Green-Lagrange strain tensor (defined in Eq. 2a) relative to the myofiber coordinate system (f = fiber direction, s = cross-fiber in-plane direction, n = transverse-fiber direction) and J is the determinant of the deformation gradient (Eq. 2b).

$$\mathbf{E} = \frac{1}{2}(\mathbf{F}^T\mathbf{F} - \mathbf{I}) \qquad\qquad\qquad (Eq.\ 2a)$$

$$J = \det(\mathbf{F}) \qquad\qquad\qquad (Eq.\ 2b)$$

Where $\mathbf{F}$ is the deformation gradient, $\mathbf{F}^T\mathbf{F}$ describe the Cauchy-Green deformation tensor and $\mathbf{I}$ is the identity tensor. The C, b_f, b_t, and b_{fs} are the diastolic material parameters; where C scales stress in all directions, b_f affects the fiber direction stiffness, b_t affects cross-fiber direction stiffness, and b_{fs} is transverse-fiber direction stiffness. The material response of the hydrogel injections was represented using a nearly incompressible, isotopic, hyperelastic constitutive law, which was defined using the following strain energy function:

$$W_{injection} = \frac{E}{2(1+v)}\ \mathrm{tr}(\mathbf{E^2})\ + \frac{E}{6(1-2v)}\ \ln(J)^2 \qquad\qquad (Eq.\ 3)$$

where **E** is the deviatoric Green-Lagrange strain tensor, tr( ) is the trace operator, and ln( ) is the natural log operator. The material parameters for Young's modulus (E) were assigned based on the experimental measurements of the hydrogels, while the Poison ratio (v) was assigned a value of 0.499.

Systolic stress was modeled as the sum of the passive stress derived from the strain energy function and an active fiber directional stress component **T**$_0$ [2, 25], which was defined by a function of time, $t,$ peak intracellular calcium contraction, Ca_0, sarcomere length, l, and maximum isometric tension achieved at the longest sarcomere length T_{max} [26].

$$\mathbf{S} = \ pJ\mathbf{C}^{-1} + 2J^{-\frac{2}{3}}Dev\left(\frac{\partial \widetilde{W}}{\partial \tilde{\mathbf{c}}}\right) + \mathbf{T_0}\{t, Ca_0, l, T_{max}\} \tag{Eq. 4}$$

where $Dev()$ is the deviatoric operator.

$$\mathbf{T_0} = \ \frac{1}{2}T_{max}\frac{Ca_0^2}{Ca_0^2+ECa_{50}^2}(1 - \cos(\frac{0.25}{ml_R\sqrt{2E_{11}+1}+b} + 1)\pi) \tag{Eq. 5}$$

where m and b are constants, E_{11} is strain in the fiber direction, Ca$_0$ is peak intracellular calcium concentration, T_{max} is maximum isometric tension achieved under maximal activation, and ECa_{50}^2 is the length-dependent calcium sensitivity given by,

$$ECa_{50}^2 = \frac{(Ca_0)_{max}}{\sqrt{exp[B(l_R\sqrt{2E_{11}+1}-l_0)]-1}} \tag{Eq. 6}$$

where B is a constant, $(Ca_0)_{max}$ is maximum peak intracellular calcium concentration, l_0 is the sarcomere length at which no active tension develops, and l_R is the stress-free reference sarcomere length. The parameters T_{max} and l_R are

discussed further in the next section. However, all other material properties used for active myocardium are defined in [25].

Chapter 3   **Transmural differences in left ventricular contractility**

3.1   Introduction

Several myocardial contractility properties have been shown to vary as a function of LV location. Experimental ex-vivo studies have examined action potential morphology, Ca^{2+} dynamics, sarcomere length, and isometric force generation [2] [5-7, 27, 28]. In addition to cellular experiments, finite element (FE) modeling has been used, in combination with magnetic resonance imaging (MRI) and ventricular pressure catheterization, to assess in-vivo myocardial material properties in the LV. In these studies, numerical optimization was used to minimize the difference between the deformation field calculated from MRI and that predicted by the FE model, using the measured pressure as a boundary condition. Passive material parameters have been estimated in the LV for both healthy [29, 30] and infarcted myocardium [31, 32]. The maximum contractile force that can be generated within the remote and border zone regions of LVs with myocardial infarction was also assessed using this approach [33-35]. However, transmural variations in force generation were not examined in these studies.

The goal of the current study, therefore, was to estimate the in-vivo contractile forces generated in the sub-endocardial, mid-myocardial, and sub-epicardial regions of healthy porcine ventricles. This was accomplished by using a combination of MRI, catheterization, and FE modeling. Properties were determined by using an optimization scheme to minimize the difference between in-vivo strains and ventricular volume calculated from MRI and FE model predicted

13

strains and volume. This work was motivated by recent ex-vivo transmural measurements [7].

3.2   Method

3.2.1 *Experimental measurements*

The animals used in this work received care in compliance with the protocols approved by the Institutional Animal Care and Use Committee at the University of Pennsylvania in accordance with the guidelines for humane care (National Institutes of Health Publication 85-23, revised 1996). In order to assess regional wall deformation in healthy adult pigs (n=4; male; approximately 40 kg), 3D SPAMM (SPAtial Modulation of Magnetization) MRI was performed with simultaneous LV pressure measurements using a pressure transducer (Millar Instruments, Houston, TX) [32]. The endocardium and epicardium of the LV were contoured from the MR images at early-diastolic filling, end-diastole, and end-systole in order to generate the reference geometry and calculate LV cavity volume. In-vivo systolic strain was calculated using a custom optical flow plug-in for ImageJ to derive 3D displacement flow fields [36].

3.2.2 FE model

Each animal-specific LV FE mesh (n=4) was produced using tri-linear hexahedral brick elements (TrueGrid; XYZ Scientific, Inc., Livermore, CA). A myofiber distribution of -37° (at epicardium) to +83° (at endocardium), with respect to the circumferential direction, was used [37]. The LV wall was evenly divided into three layers: sub-epicardium, mid-myocardium, and sub-endocardium (Figure 5). The measured pressure was used as a boundary condition to simulate end-diastole and end-systole.

The material behavior for passive myocardium was considered as hyperelastic, nearly incompressible, and transversely isotropic with respect to the local myofiber direction. The strain energy function is defined in Eq. 1. The diastolic material parameters were determined in a previous study for each animal and incorporated into the animal-specific FE models [32]. Systolic stress was modeled as the sum of the passive stress derived from the strain energy function and an active fiber directional stress component T_0 (Eq. 3) [2, 25]. Note the one of the key parameters used to describe active stress is T_{max}, which represents the maximum isometric force that can be generated by a myocyte. Each FE simulation was conducted in two phases, where the first phase represented passive diastolic filling and the second phase represented active systolic contraction to end-systole (LS-DYNA, Livermore Software Technology Corporation, Livermore, CA).

3.3   Optimization procedure

The primary focus of the optimization was to determine the distribution of T_{max} within the LV wall. The optimization process was performed using the software LS-OPT (Livermore Software Technology Corporation, Livermore, CA) as previously described [31]. Briefly, the genetic algorithm (GA) technique was used to minimize the objective function, which was taken to be the mean squared error (MSE) between experimentally measured data and FE predicted results, and was defined as

$$MSE = \sum_{n=1}^{N} \sum_{i,j=1,2,3} \left(E_{ij,n} - \bar{E}_{ij,n} \right)^2 + \left(\frac{V - \bar{V}}{\bar{V}} \right)^2 \qquad \text{(Eq. 6)}$$

where n is the strain point within the myocardium, N is the total number of strain points, $E_{ij,n}$ and V are the FE predicted end-systolic strain and LV cavity volume, respectively (over bar variables represent in-vivo measured values). A total of N=756 points evenly distributed throughout the FE model were compared to the nearest LV points from the MRI-derived strain data. Specifically, the points were selected at the element centroids in a pattern of 3 transmural x 36 circumferential x 7 longitudinal points. Over the LV wall, this yielded 252 points per transmural layer. The search range for the parameter T_{max} was 40 kPa to 400 kPa based on previous studies [33, 34, 38, 39]. In order to determine the transmural distribution of T_{max}, in combination with different transmural distributions of l_R, four cases were tested with the aforementioned optimization procedure (Table 1). Once each optimization was fully converged, the 95% confidence intervals were calculated for

the last iteration of each case. The intervals were based on the parameters used to generate the 64 simulations that were run during the last iteration and represent the range over which the optimization is 95% confident that the parameter values exist.

3.4   Results

All of the optimizations converged to the final set of T_{max} parameters after 15 generations of the GA. The values of T_{max} optimized for each case are shown in Tables 2-5 along with their respective 95% confidence intervals. Notably, as compared to Case 1 (Table 2) where both l_R and T_{max} were uniformly distributed, inclusion of transmural variations in either l_R (Case 2; Table 3) or T_{max} (Case 4; Table 5) led to a smaller MSE value in all four animals; the MSE values decreased by 13% and 15% in Case 2 and Case 4, respectively, on average. Inclusion of transmural variations in both l_R and T_{max} as in Case 3 further decreased the averaged MSE value by 22% as compared to Case 1 (Table 2 vs. Table 4). Interestingly, in both Case 3 and Case 4, most of the animals (3 out of 4) exhibited higher T_{max} in the mid-myocardium as compared to the values in the sub-epicardium and sub-endocardium (Tables 4 and 5, Figures 6 and 7). On average, T_{max} generated in the mid-myocardium was more than 1.7 times of that produced in the other layers in these two cases.

The transmural distribution of systolic strain components (circumferential, longitudinal, and circumferential-longitudinal shear) in the LV free wall was investigated more closely for Case 1 and Case 3, which exhibited the highest and

17

lowest MSE value, respectively. Both Case 1 and Case 3 exhibited a non-uniform distribution of systolic strain similar to the experimental data (Figure 8). Moreover, the sub-endocardium consistently exhibited the largest magnitude of systolic strain. Results of Case 3, however, showed better agreement with the experiment measurements as compared to those of Case 1. Specifically, the systolic strain distribution from Case 3 was within the 95% confidence interval of the experimentally measured strain components, whereas Case 1 fell outside of the intervals (Figure 8). The value of the objective function was also assessed within each transmural layer for Case 1 and Case 3. The value of MSE in the sub-epicardium, mid-myocardium, and sub-endocardium was 17.33, 14.45, 36.83 for Case 1, respectively, and 16.5, 13.3, 23.6 for Case 3, respectively. The fit between the experimental and FE calculated results was improved in all three transmural layers for Case 3. Most notably, the value of MSE was decreased by 35% in the sub-endocardial layer, which showed the most improvement in the fit.

In order to assess the influence of non-uniform contractility and reference sarcomere length on LV torsion, the twist angle at the apex of the FE models was calculated in each of the 4 cases (Figure 9). These calculations were performed using the approach outlined in [19]. The results indicate that Case 3 produced the largest twist angle, compared to the other cases. More specifically, when comparing Case 2 and Case 3, which have the same non-uniform distribution of l_R but different distributions of T_{max}, it can be seen that a uniform distribution of T_{max} produced a twist angle of 11.5 degrees (Case 2) compared to a non-uniform distribution, which produced a twist angle of 16.3 degrees (Case 3). Interestingly,

when comparing Case 4 and Case 3, which both have non-uniform distributions of T_{max} but different distributions of l_R, it can be seen that a uniform distribution of l_R produced a twist angle of 12.2 degrees (Case 4). This implies that the distribution of T_{max} has more of an effect on the twist angle than the distribution of l_R. When both T_{max} and l_R were assumed to be uniform (Case 1), LV twist angle was at a minimum with a value of only 9 degrees.

3.5   Discussion

The goal of the current study was to estimate the transmural distribution of in-vivo myocardial contractile force using a combination of MRI, catheterization, FE modeling, and numerical optimization. For this purpose, the maximum isometric tension, T_{max}, was investigated particularly because it is one important determinant of cardiomyocyte contractility. A recent ex-vivo study has shown that maximum isometric force generation exhibits transmural heterogeneity in healthy human hearts [7]. Consistent with these results, the current study showed that when the same level of T_{max} is used in all three transmural regions, the MSE values are much larger than those with a non-uniform distribution. This indicates that the strain field in a model with non-uniform contractility distribution is more representative of the deformation that occurs in-vivo. In support of this, the model with transmural variations in T_{max} exhibited better agreement with the in-vivo experimental measures in terms of systolic strains. Recently, a sensitivity study was performed, which evaluated the influence of different transmural distributions of contractile force, and showed that the transmural distribution affects LV deformation via

altered torsion [40]. This may, at least in part, explain the better fit exhibited by models assuming a non-uniform contractility distribution across the LV wall. Moreover, in the current study the fit was further improved by incorporating a non-uniform transmural distribution of the reference sarcomere length, which represents a more realistic morphology of the LV.

Interestingly, with this more representative FE model of the LV, the mid-myocardium from most of the animals tested in the current study exhibited the highest contractile force, which was followed by the sub-epicardium and sub-endocardium, in terms of T_{max}. Although these results were not associated with statistical significance, they show strong agreement with the recent ex-vivo experimental results of [7]. In addition, previous studies have reported that the epicardium contracts slightly more than the endocardium, which is consistent with our study results [5, 6]. Finally, consistent with previous studies [41-43], the systolic strain components exhibited transmural variation, where the highest magnitude occurred at the endocardial surface and the lowest at the epicardial surface.

In order to more directly assess changes in LV torsion, the apical twist angle was measured in each of the models. It was found that a non-uniform distribution of T_{max} produced the largest value of twist angle compared to the cases with a uniform distribution. This implies that transmurally varying contractile properties could be a key factor in maximizing LV torsion. Although residual stress was not included in the model, the non-uniform transmural distribution of the reference sarcomere length incorporates an important factor that influences systolic function. This, together with transmurally varying contractility, may serve to homogenize the

force generation during LV systole for an optimal pump function. In addition, changes in the magnitude of the active stress in the cross-fiber direction also impacted the fitness of FE models to experimental data (data not shown). Again, in these cases, models assuming transmurally varying T_{max} and l_R provided the best fit.

It should be noted that the contribution of the relative volume change to the MSE calculation was much less than the contribution of the strain. In all of the cases, the LV volume in the model was within 5% of the experimentally measured value. This implies that all the converged models matched the end-systolic volume very closely. Therefore, when comparing the MSE values of all the cases, the differences are primarily attributed to the model fit to the experimental strain. For example, comparing the average MSE for Case 1 (68.65) to that of Case 3 (53.47) implies that the decrease in MSE is caused by a better fit to the experimental strain data when using a heterogeneous sarcomere length and isometric tension distribution.

The model-predicted longitudinal strain showed greater shortening than the experimental strain, whereas the circumferential strain showed less shortening than the experimental strain. This effect in the model could explain the discrepancy between the model cases and the experimental strain (Figure 8). This result could be affected by the fiber angle distribution, which was based on histology rather than diffusion tensor MRI data (since it was not available), the assumption of transverse isotropy, or the level of cross-fiber contraction. These limitations will be addressed in future studies.

3.6   Conclusion

In conclusion, the current study showed that a non-uniform transmural distribution of myocardial contractile force produced the best agreement between in-vivo measured strain from MRI and that predicted by the FE model. More experiments are needed to confirm the in-vivo results of the current study. Despite the limited statistical power due to the small sample size (n=4), the results support recent experimental ex-vivo measurements on cardiomyocytes [7], which showed that the mid-myocardium generates the greatest force. Since heart disease has recently been associated with altered myocardial contractility in specific transmural regions [7], the incorporation of transmural variation of active properties, therefore, may provide a better representation of how disease alters LV function.

Table 1 Description of 4 cases used in the optimization of transmural contractility.

Cases	Description
Case 1	l_R was assigned as 1.85 μm in all three myocardial layers, and T_{max} assumed the same value throughout the LV wall during optimization
Case 2	l_R was assigned as 1.91 μm, 1.85 μm, and 1.78 μm in the sub-epi-, mid-, and sub-endo-myocardium, respectively, and T_{max} assumed the same value throughout the LV wall during optimization
Case 3	l_R was assigned as 1.91 μm, 1.85 μm, and 1.78 μm in the sub-epi-, mid-, and sub-endo-myocardium, respectively, and T_{max} was allowed to vary in all three LV layers during optimization
Case 4	l_R was assigned as 1.85 μm in all three myocardial layers, and T_{max} was allowed to vary in all three LV layers during optimization

Note: Transmural distributions of reference sarcomere lengths are based on measurements of unloaded rat LV taken from [44].

Table 2 Transmural distribution of maximum isometric tension (Tmax; kPa) in Case 1.

Animal	Maximum isometric tension ± 95% confidence interval			MSE
	sub-epicardium	mid-myocardium	sub-endocardium	
1	84.93 ± 4.30	84.93 ± 4.30	84.93 ± 4.30	89.33
2	97.13 ± 4.83	97.13 ± 4.83	97.13 ± 4.83	66.34
3	76.45 ± 3.51	76.45 ± 3.51	76.45 ± 3.51	57.70
4	182.00 ± 10.66	182.00 ± 10.66	182.00 ± 10.66	61.21
Mean	110.13			68.65

Note: Case 1: uniformly distributed reference sarcomere length across the LV wall.

Table 3 Transmural distribution of maximum isometric tension (Tmax; kPa) in Case 2.

Animal	Maximum isometric tension ± 95% confidence interval			MSE
	sub-epicardium	mid-myocardium	sub-endocardium	
1	80.13 ± 3.18	80.13 ± 3.18	80.13 ± 3.18	65.45
2	97.05 ± 4.93	97.05 ± 4.93	97.05 ± 4.93	63.65
3	75.17 ± 3.03	75.17 ± 3.03	75.17 ± 3.03	52.20
4	169.30 ± 8.63	169.30 ± 8.63	169.30 ± 8.63	57.20
Mean	105.41			59.60

Note: Case 2: transmurally varying reference sarcomere length.

Table 4 Transmural distribution of maximum isometric tension (Tmax; kPa) in Case 3.

Animal	Maximum isometric tension ± 95% confidence interval			MSE
	sub-epicardium	mid-myocardium	sub-endocardium	
1	118.10 ± 3.63	63.08 ± 2.18	60.88 ± 2.45	51.61
2	86.48 ± 3.49	140.80 ± 5.36	51.22 ± 2.14	60.49
3	76.17 ± 3.31	83.92 ± 3.87	51.10 ± 2.55	48.00
4	148.10 ± 4.83	254.30 ± 6.32	72.72 ± 3.76	53.78
Mean	107.21	135.53	58.98	53.47

Note: Case 3: transmurally varying reference sarcomere length.

Table 5 Transmural distribution of maximum isometric tension (Tmax; kPa) in Case 4.

Animal	Maximum isometric tension ± 95% confidence interval			MSE
	sub-epicardium	mid-myocardium	sub-endocardium	
1	102.70 ± 4.55	78.80 ± 3.14	50.02 ± 1.96	61.49
2	50.08 ± 2.25	199.0 ± 6.53	102.40 ± 3.32	62.56
3	79.24 ± 3.25	90.93 ± 4.19	50.29 ± 3.41	53.28
4	173.50 ± 5.08	290.10 ± 7.65	81.60 ± 3.93	56.77
Mean	101.38	164.71	71.08	58.50

Note: Case 4: uniformly distributed reference sarcomere length across the LV wall.
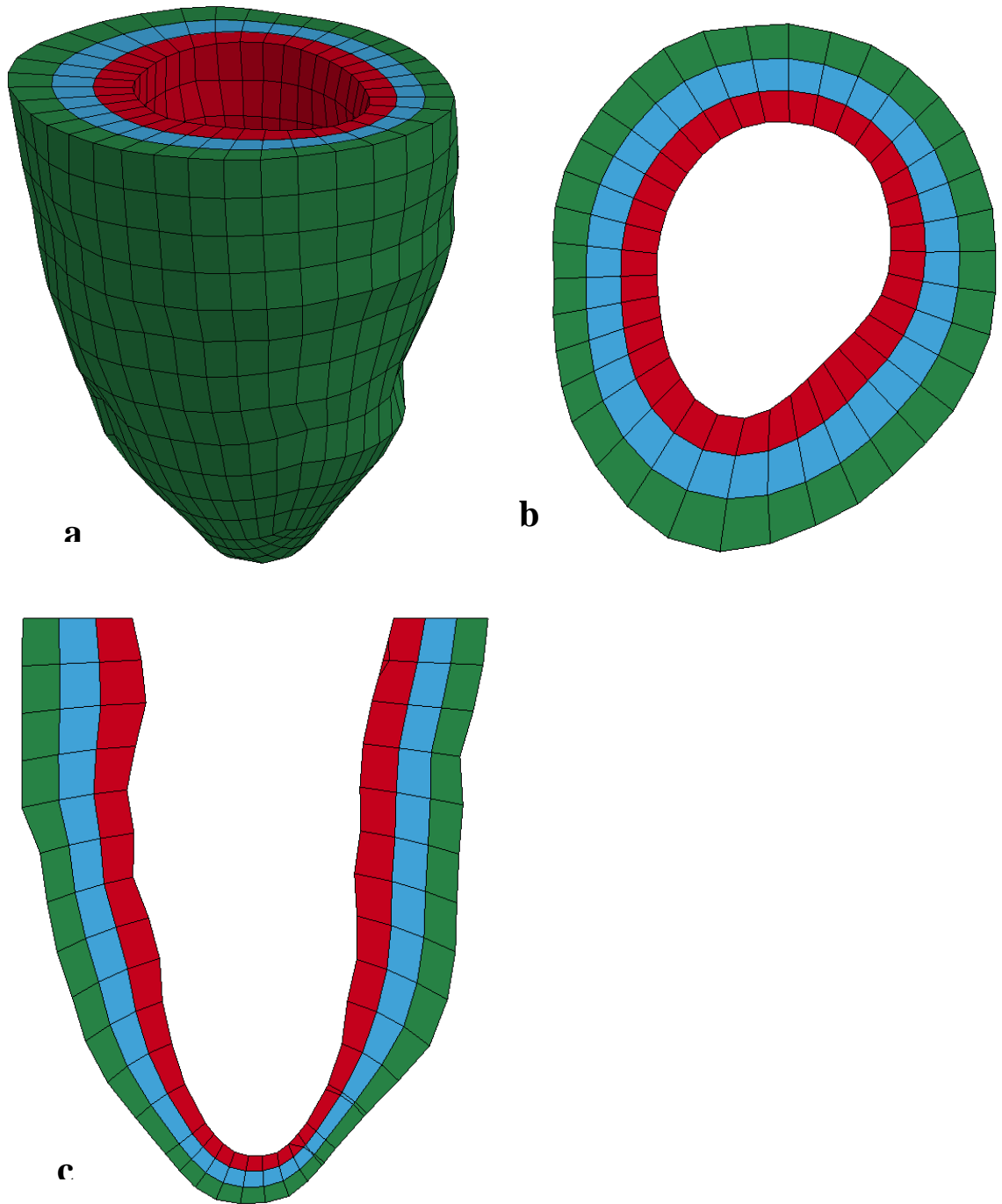
Figure 5 Representative animal-specific FE model of a porcine LV with 3 transmural layers. (a) 3D view; (b) short axis view; (c) long axis view.
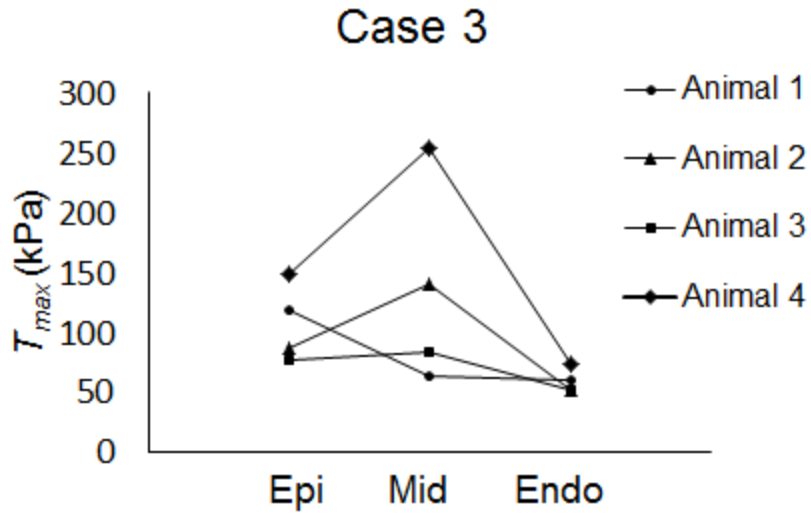
Figure 6 Visual representation of transmural distribution of maximum isometric tension in Case 3.
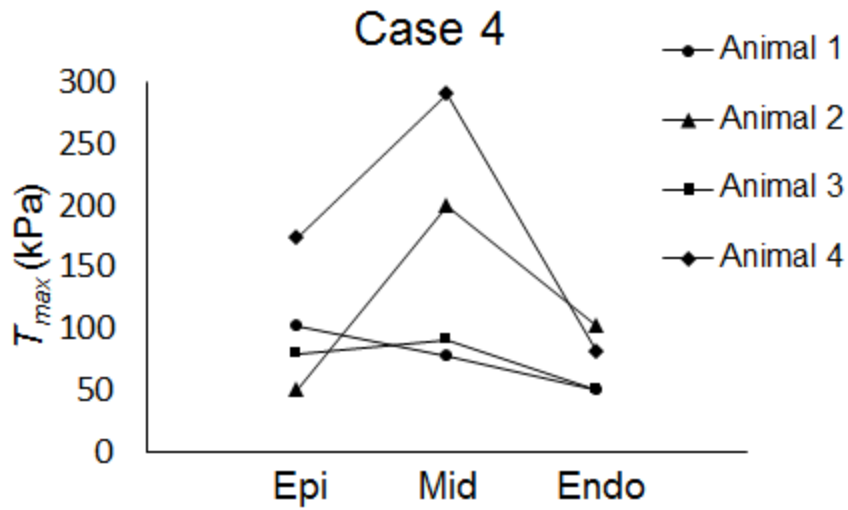
Figure 7 Visual representation of transmural distribution of maximum isometric tension in Case.
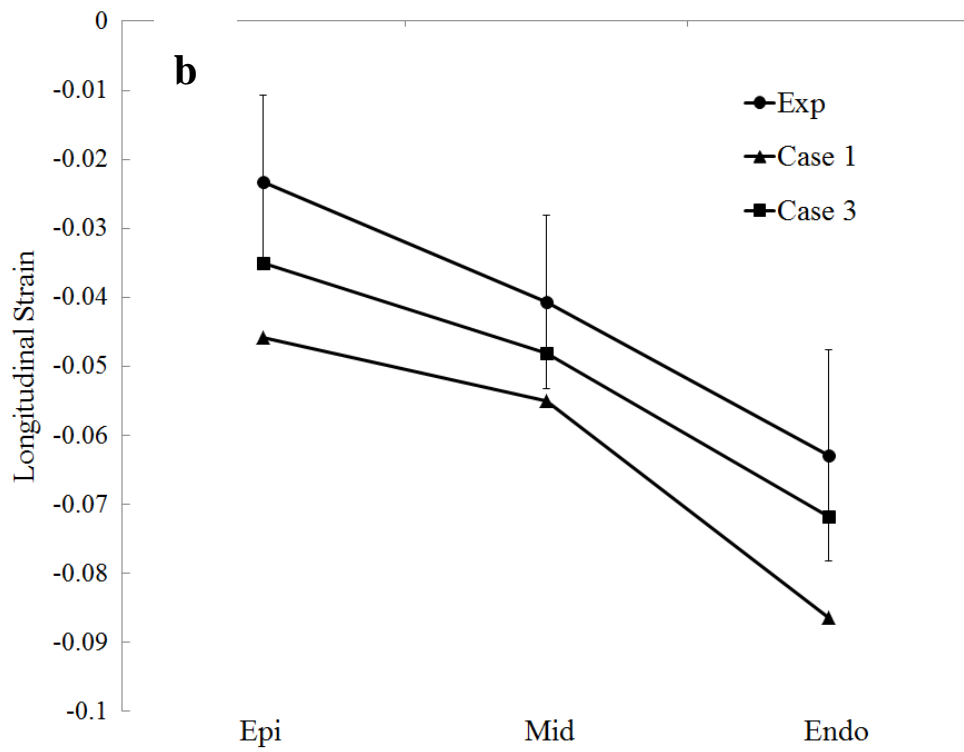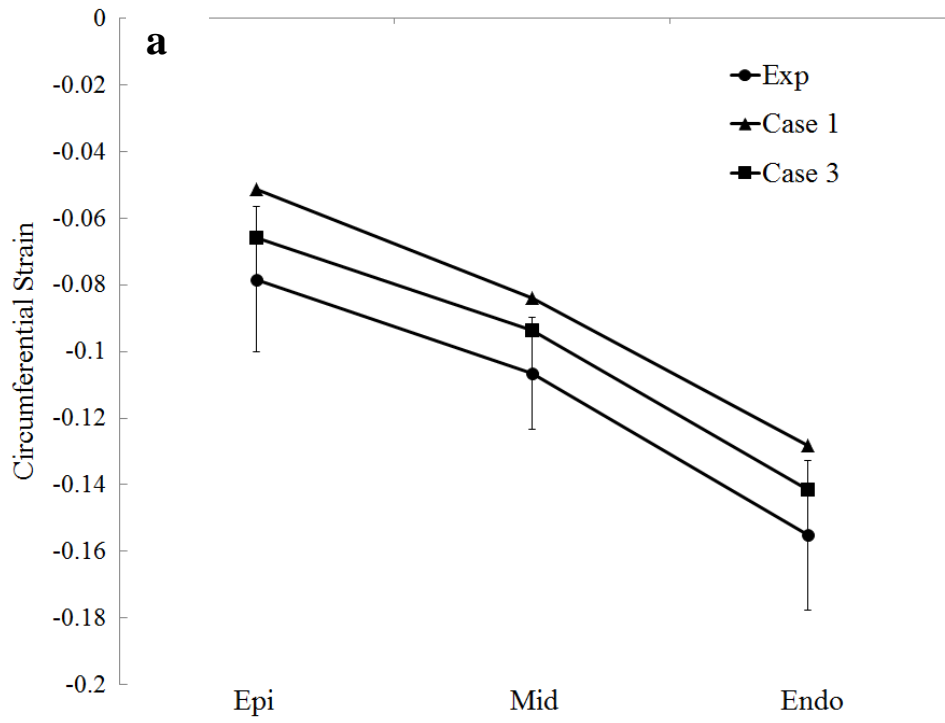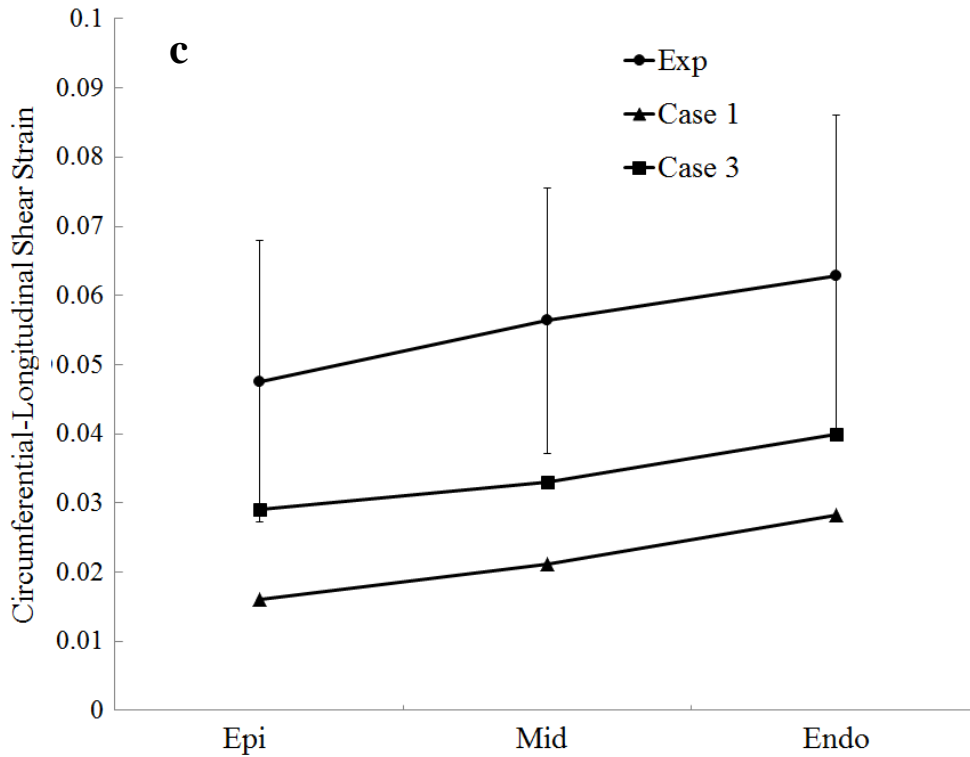
Figure 8 Transmural distribution of (a) circumferential, (b) longitudinal, and (c) circumferential-longitudinal strain at end-systole in the LV free wall. Case 1: uniformly distributed reference sarcomere length and maximum isometric tension; Case 3: transmural varying reference sarcomere length and maximum isometric tension.
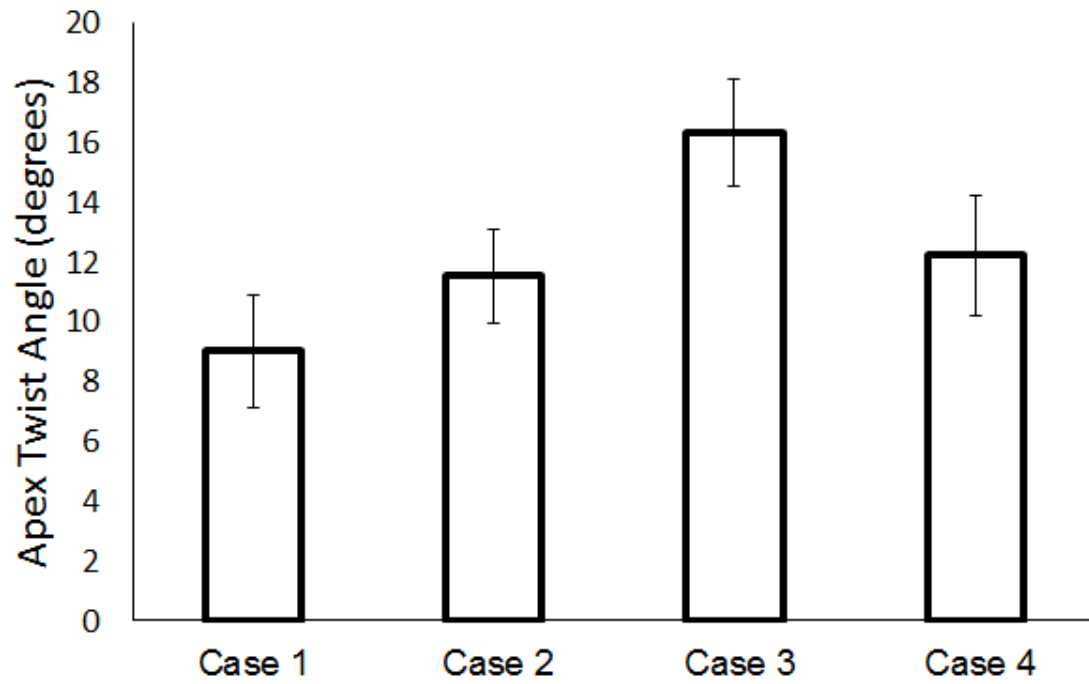
Figure 9 Apex twist angle (degrees) calculated in the FE models for each of the cases. Values were mean ± SEM; n = 4 animals.

Chapter 4   **Sensitivity study of hydrogel injection characteristics for myocardial support**

This study is a continuation of previous work done in collaboration with the University of Pennsylvania, which sought to evaluate the efficacy of two different hydrogels for treating myocardial infarction in ovine infarct heart and explores the fact that the stiffness of these injections can be tuned to minimize wall thinning and ventricular dilation [24].

4.1   Introduction

The material properties of myocardium are an important determinant of global LV function in both health and disease. One potential treatment strategy being investigated is the use of biocompatible injectable materials as a means of augmenting MI mechanics. Several formulations of injectable biomaterials have been studied using animal models to evaluate the impact on wall thickness and global LV function [45-48]. These in vivo studies have demonstrated that injectable hydrogel injections can mitigate the adverse effects of MI [24, 48].

Interestingly, the stiffness of these injections can be tuned to minimize wall thinning and ventricular dilation. Specifically, work done by Rodell et al. tested two different hydrogel injections with altered stiffness characteristics, namely, one with a higher stiffness (41 kPa) called dual-crossing (DC) and another with a lower stiffness (0.8 kPa) called gust-host (GH) [24]. This study aims to evaluate the efficacy of these two different hydrogels for treating myocardial infarction in ovine

heart, compared to control injection case. There are three separate groups: MI control with saline injection, MI treatment with soft hydrogel, MI treatment with stiffening hydrogel used in this study. The study is summarized below.

The LV myofiber stress distribution around the GH and DC hydrogel injections is shown in Figure 10A and 10B, along with the transmural distribution of stress between injections (Figure 10C). The DC hydrogel reduced the myofiber stress by roughly 36% at the epicardium, 14% at mid-myocardium, and 43% at endocardium compared to the control case (Figure 10C) [24]. However, the GH hydrogel case showed almost no change in the transmural distribution of myofiber stress compared to the control case. Additionally, the average myofiber stress in the myocardium surrounding the DC injection was 2.5 kPa (26% reduction compared to control) and the stress around the GH injection was 3.4 kPa (0% reduction compared to control) [24]. This is primarily driven by the fact that the DC injections maintained their original shape (due to material stiffness), which allowed the LV wall to remain thick (Figure 10B). However, it can be seen that the GH injections effectively collapse as the LV wall is loaded by the pressure on the endocardium (Figure 10A). More specifically, the average wall thickness at end-diastole for the control case was approximately 1 cm, while the thickness for the GH case was 1.08 cm and the DC case was 1.23 cm [24].

The results showed a better ability to limit infarct expansion and remodeling with the higher stiffness hydrogel injection. Inspired by that study, the current investigation combines experimental data and finite element (FE) modeling to better understand how hydrogel injection stiffness and volume influence

myocardial wall stress and wall thickness. This was accomplished by using previously measured MRI data from explanted ovine LVs, which were injected with an array of hydrogel, in order to assess injection geometry. FE models were then constructed to represent various combinations of injection volume within the LV wall, over a range of hydrogel elastic moduli.

4.2   Method

4.2.1 Finite Element Model

In order to evaluate the effects of various hydrogels, FE models of the LV with two different injection volumes (150 µL and 300 µL) were generated, as well as a control model with no injections. The reference configuration of each model was chosen to represent early diastole, since the stress in the LV is at a minimum. The LV FE meshes were produced using tri-linear hexahedral brick elements (TrueGrid; XYZ Scientific, Inc., Livemore, CA). The size and shape of the hydrogel injections were based on MRI reconstruction of injected explant tissue (Figure 11 12, Table 7) [24, 49]. The geometry of the LV wall was based on experimental measurements from the ovine hearts [24]. For the control case, the undeformed wall thickness was approximately 1.3cm, the inner diameter of the endocardial wall near the equator was 4 cm, and the distance from base to apex was 6.4 cm.

For the models with hydrogel injections, the control model was modified to include a 4 x 4 pattern of 16 injections within the myocardium and the spacing between injections was assumed to be 1.5 cm from center to center (Figure 13a) [24, 49, 50]. Since the injections remain as discrete plugs in the LV wall, rather

than diffusing into the tissue, the total volume of myocardium must be conserved. This was accomplished by increasing the wall thickness in the injection region within each FE model. For the case of 300 µL injections, the wall thickness was increased by 1.5 mm to account for the volume added to the wall (Figure 13b). For the case of 150 µL injections, the wall thickness was increased by 0.5 mm (Figure 13c). The LV wall away from the injections, and the longitudinal dimensions, were unaltered relative to the control case. The myofiber orientation was assigned to vary linearly from epicardium to endocardium using the angle of -37 degrees to 83 degrees, respectively [37]. A pressure of 10 mmHg was assigned as a boundary condition on the endocardial surface in each of the FE models, in order to simulate end-diastole.

4.2.2 Material response

The material response of the myocardium was represented using a nearly incompressible, transversely isotropic, hyperelastic constitutive law, which was defined in Eq1. The diastolic material parameters were assigned to be C=0.51 kPa, b_f =22.84, b_t =3.45, and b_{fs} =12 [51], while the bulk modulus was κ = 1e10^3 kPa.

The material response of the hydrogel injections was represented using Eq 3. The material parameters for Young's modulus (*E*) were assigned in a range between 0.1 kPa to 100 kPa, while the Poison ratio (*v*) was assigned a value of 0.499. The range for Young's modulus was based on measurements by Rodell et al. [24], where two formulations with a modulus of 0.8 kPa and 41 kPa were injected into an ovine model of MI.

4.3   Results

End-diastolic myofiber stress was assessed along the transmural direction, in between injections, for the different stiffness cases. Figure 13a shows that when the injection stiffness is 0.1 kPa the transmural distribution of stress is nearly unchanged compared to the untreated control. For a hydrogel stiffness of 25 kPa, the 150 µL injection reduced the myofiber stress by roughly 18.9% at the epicardium, 0% at mid-myocardium, and 21.6% at endocardium compared to the control (Figure 14b). While, the 300 µL injection reduced the myofiber stress by roughly 31% at the epicardium, 10.6% at the mid-myocardium, and 34.7% at the endocardium compared to the control (Figure 14b). For a hydrogel stiffness of 100 kPa, the 150 µL injection reduced the myofiber stress by roughly 39.2% at the epicardium, 18.3% at mid-myocardium, and 38.7% at the endocardium compared to the control (Figure 14c). While, the 300 µL injection reduced the myofiber stress by roughly 56.8% at the epicardium, 36.5% at the mid-myocardium, and 55.2% at the endocardium compared to the control (Figure 14c).

Additionally, the average myofiber stress in the myocardium surrounding the 150 µL and 300 µL injections, using different hydrogel stiffness values, is shown in Figure 15. When the injection stiffness is increased, the myofiber stress was decreased. It should be noted that the influence of stiffness begins to level off after 50 kPa. Figure 16 shows the average wall thickness as a function of injection stiffness. When the injection stiffness increased, the wall thickness was increased. The average wall thickness at end-diastole for the control was approximately 1cm,

while the thickness for the 150 µL injection with 25 kPa stiffness was 1.1cm and 300 µL was 1.2cm. For the case of 150 µL injection with 100 kPa stiffness, the thickness was 1.2cm, while 300 µL was 1.3cm. This is primarily driven by the fact that the stiffer injections maintained their original shape during deformation, which allows the LV wall to remain thick (Figure 17c and 17f). On the other hand, it can be seen that the 0.1 kPa injections effectively collapse in the transmural direction as the LV wall is loaded by the pressure on the endocardium (Figure 17a and 17d). Figure 17 also shows the distribution of end-diastolic myofiber stress throughout the LV wall around the 150 µL injections (Figure 17 a-c) and 300 µL injections (Figure 17 d-f), with stiffness values of 0.1 kPa, 25 kPa and 100 kPa, respectively. It is clear that the myofiber stress showed a greater reduction around the hydrogel injection region when the volume was larger and the stiffness was higher.

4.4   Discussion

The goal of the current study was to assess the effect of different attributes that can be tuned for hydrogel injections. More specifically, this work utilized a combination of previously measured MRI data and FE modeling to investigate how injection stiffness and volume influence myocardial wall stress and wall thickness. The modeling results show a clear reduction of myofiber stress based on the higher hydrogel injection volume. Additionally, by turning the stiffness of the hydrogel, greater reductions in stress can be achieved. The current results indicated that stiffer hydrogel injections could reduce myofiber stress further. These improvements appear to taper after a stiffness of 50 kPa.

Previous studies have used FE modeling to assess the influence of biomaterial injections on LV function and wall stress. Kichula et al. [51] examined the effects of a single hydrogel formulation, which diffused between the tissue, and a single injection volume on LV wall stress. It was found that the injections increased the effective stiffness of the tissue and decreased stress in the wall. Two other studies examined the effects of varying the volume of the injections on wall stress and LV ejection fraction, but did not examine the effects of injection stiffness. Lee et al. [52] used a patient-specific FE model to show that increasing the injection volume decreased both the end-diastolic and end-systolic stress in the myocardium. Wise et al. [53] used an animal-specific FE model of a rat heart to investigate a wide range of injection volumes in a model of MI. Interestingly, it was found that the beneficial effects of the injection began to diminish once the volume fraction of the injection exceeded 50% of the MI region. It should be noted that the volume fraction of hydrogel injection to treated myocardium in the current study was less than 15%. Also, the results of the current study were consistent with these previous studies, in terms of decreasing myofiber stress with increased injection volume. However, the current study showed the additional benefit of tuning the injection stiffness to reduce stress.

In addition to FE modeling studies, several experimental studies with large animal models have been conducted. Ifkovits et al. found that stiffer hydrogel injections led to a reduction in adverse remodeling in the MI region, i.e., the MI region was smaller in animals treated with stiffer hydrogels, compared with the control infarct group [45]. In work done by Plotkin et al., it was shown that

hydrogels with the highest stiffness exhibited the best rescue of heart function [54], in terms of ejection fraction. Also, in another previous experiment study, it was shown that the higher stiffness hydrogel injection improved the ejection fraction after 8 weeks but not the lower stiffness hydrogel injection; and LVEDV measured using the higher stiffness hydrogel was smaller than the lower stiffness hydrogel [24]. All of these experimental studies showed greater benefit with a higher stiffness hydrogel, in terms of better LV geometry and function. This is consistent with the current FE modeling results, which indicate that the higher stiffness hydrogel injections are more beneficial. Additionally, previous injectable biomaterial studies have demonstrated that injections can increase LV wall thickness and the effective stiffness of the infarct region [45, 46, 50, 55-57]. This is also consistent with the current results, in which a higher injection stiffness led to increased wall thickness due to better retention of injection shape.

4.5 Conclusion

In the current work, FE modeling was used to predict how the LV wall thickness and myofiber stress change as a function of different hydrogel characteristics. This approach could be used as a tool for developing tunable hydrogel injections and predicting stress reduction and heart function post-MI. In the future, this method will be used to examine more optimal injectable biomaterial properties, which would be valuable clinical treatments for treat myocardial infarction.

Table 6 Ellipsoidal dimensions of the 150µL hydrogel injection and 300µL hydrogel injection, based on MRI data.

	150 µL	300µL
a	5.50 mm	6.60 mm
b	3.15 mm	3.94 mm
c	2.40 mm	2.73 mm

A   B
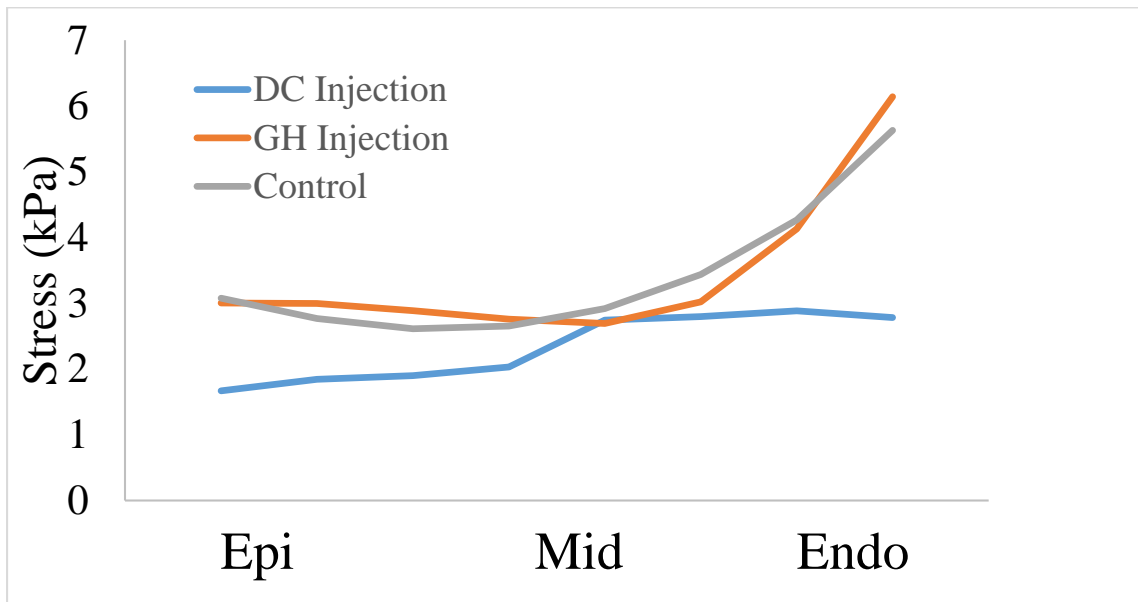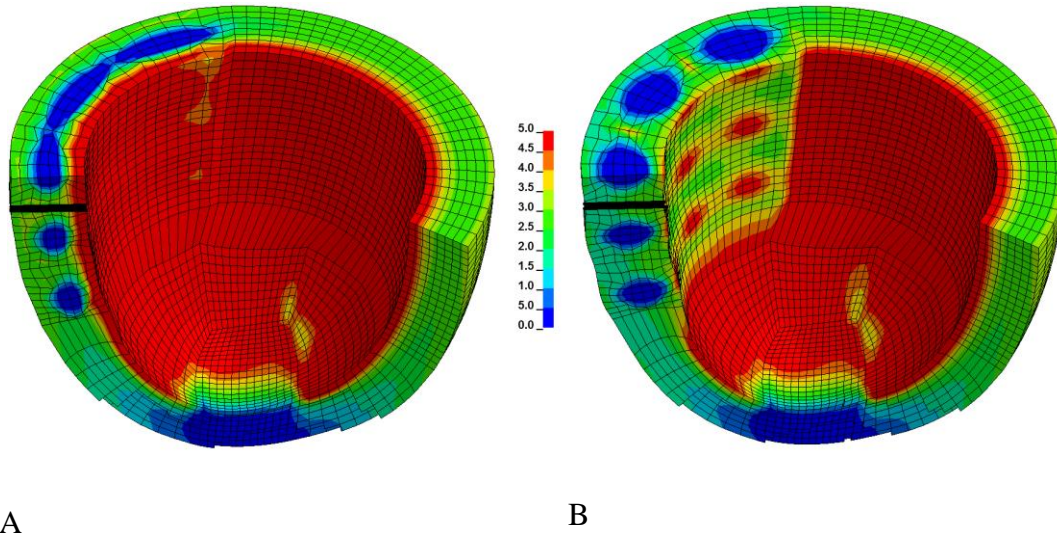
C

**Figure 10 End-diastolic myofiber stress (kPa) distribution for an LV with (A)
GH hydrogel injections and (B) DC hydrogel injections. Note that only a
quarter of the model is shown in order to visualize the distribution within the
myocardium. (C) Transmural fiber stress distributions for three cases [24].**
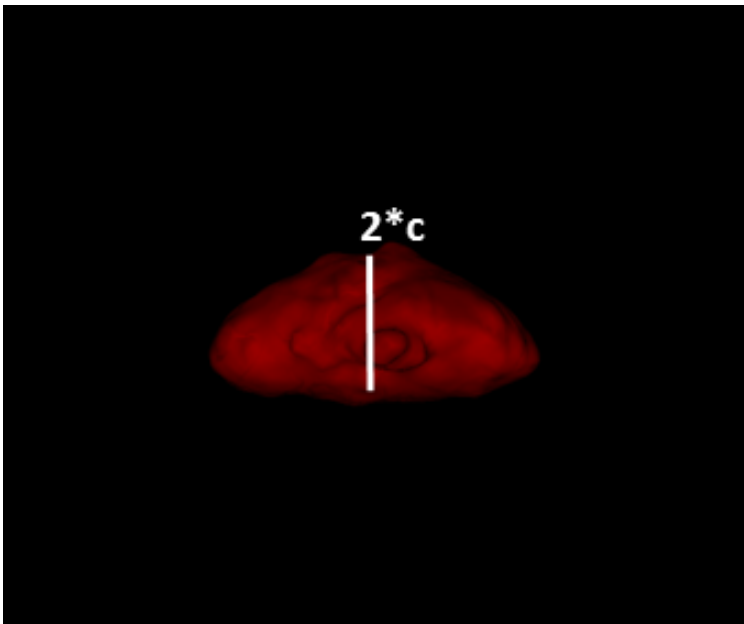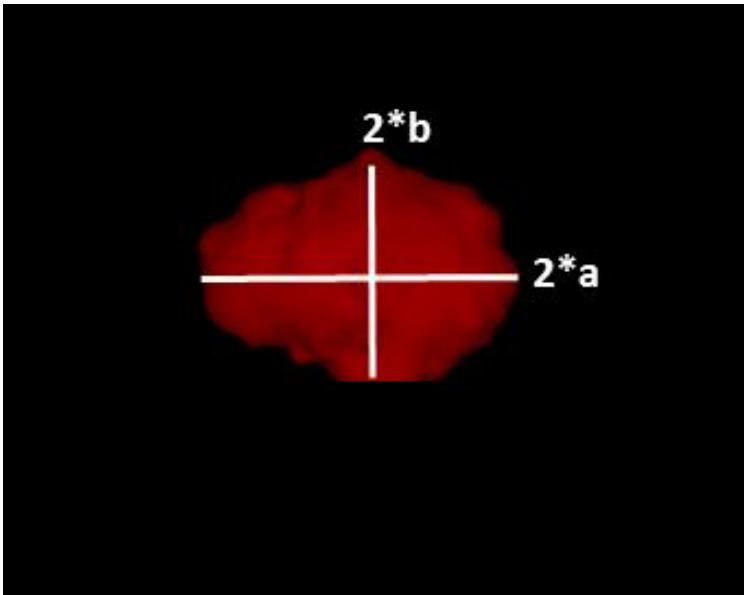
Figure 11 Reconstruction of hydrogel geometry based on MRI data of injections embedded in myocardial wall. Note that the shape is approximately ellipsoidal [24].
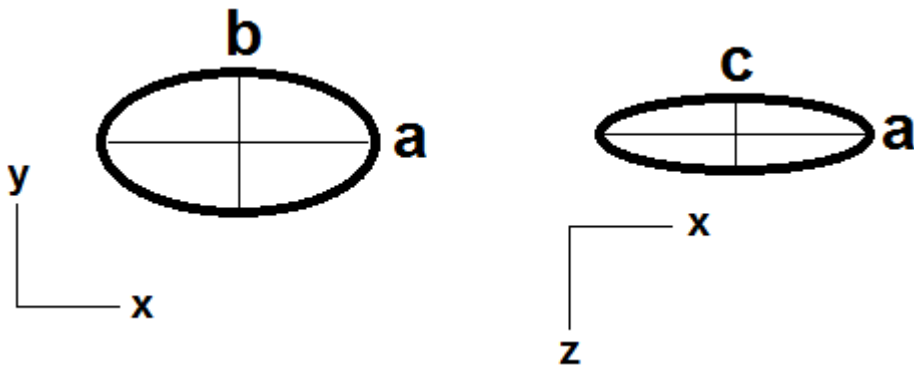
Figure 12 Hydrogel injections are well retained and can be approximated as an ellipsoid with characteristic dimensions a, b, and c.
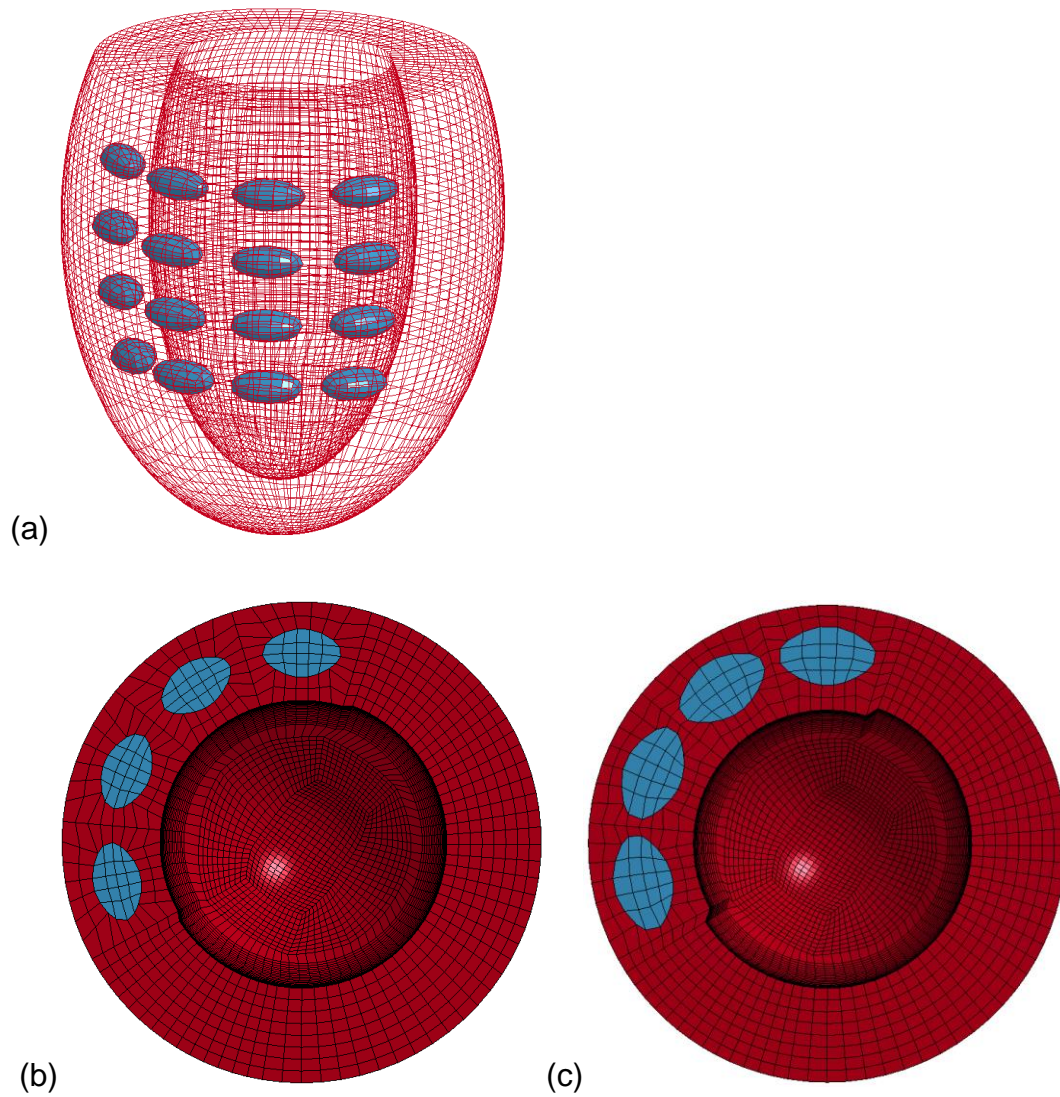
Figure 13 (a) FE model of an ovine LV with 16 150 μL hydrogel injections. (b) Short axis view of the LV wall with 150 μL hydrogel injections. (c) Short axis view of the LV wall with 300 μL hydrogel injections.
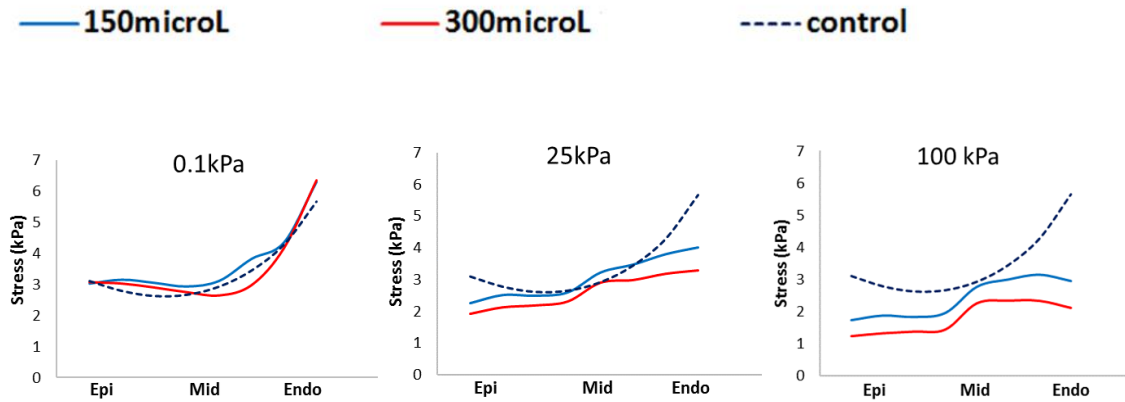
Figure 14 (a-c) End-diastolic transmural distribution of myofiber stress using stiffness 0.1kPa, 25kPa and 100kPa hydrogel injection between 150µL injection and 300µL injection.
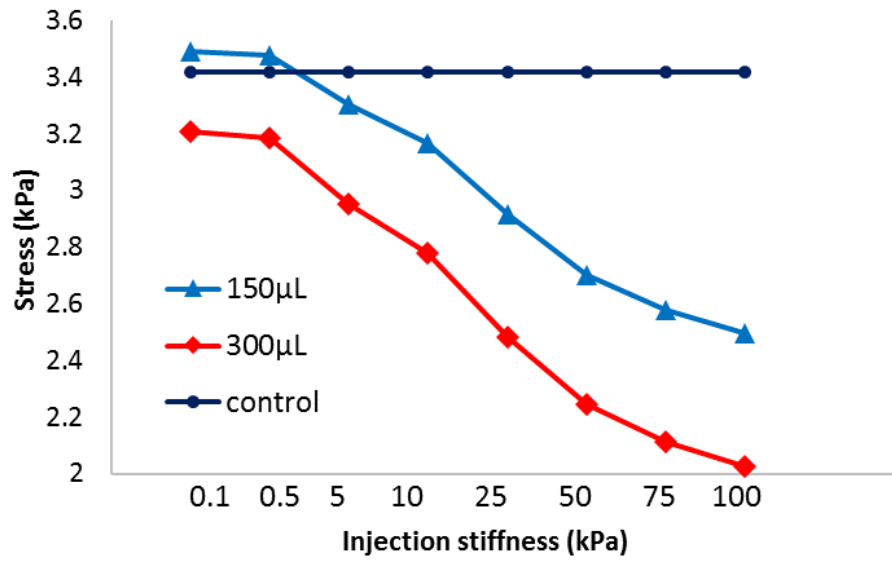
Figure 15 Average end-diastolic myofiber stress surrounding the injection as a function of injection stiffness and volume.
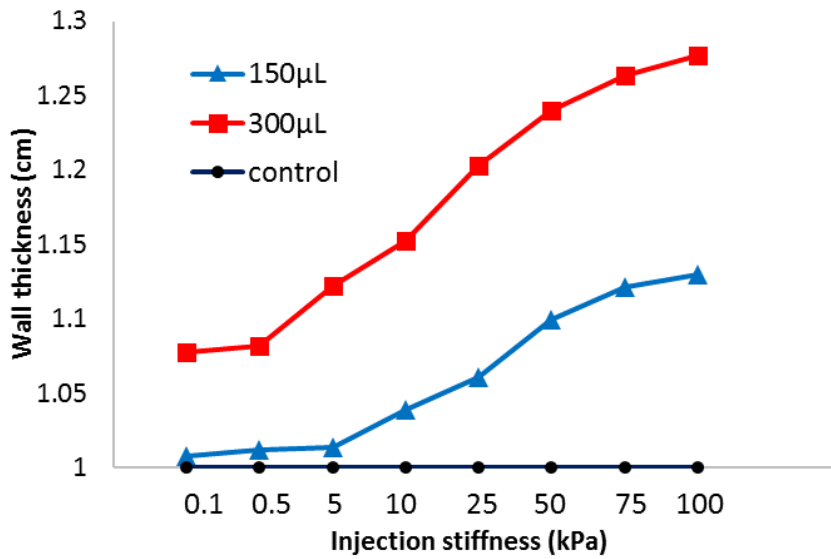
Figure 16 End-diastolic myocardial wall thickness in the injection region as a function of injection stiffness and volume.
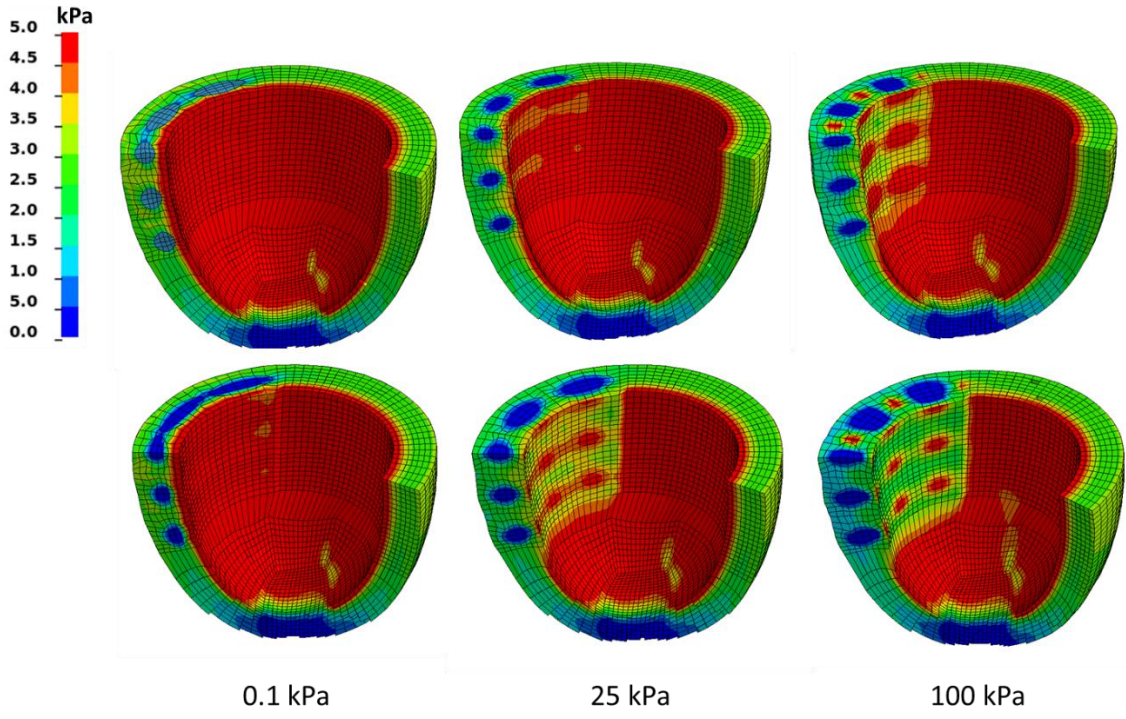
Figure 17 (a-c) The LV myofiber stress distribution around 150μL injections and (d-f) 300μL injections with stiffness values of 0.1kPa, 25kPa and 100kPa.

Chapter 5   **Effects of Hydrogel Injection on Borderzone Contractility Post Myocardial Infarction**

5.1   Introduction

Early infarct expansion or stretching has been associated with poor long-term prognosis [13-15] and has been identified as the mechanical phenomenon that initiates and sustains the process of adverse post-MI LV remodeling that leads to heart failure [16-21]. Infarct expansion causes abnormal stress distribution in myocardial regions within and outside the MI, especially in the adjacent normally perfused borderzone (BZ) region. With time, increased regional stress is the impetus for maladaptive biologic processes, such as matrix metalloproteinase activation, that inherently alter the contractile properties of normally perfused myocardium [22]. Once initiated, these maladaptive processes lead to a heart failure phenotype that is difficult to reverse by medical or surgical means.

It has been demonstrated that externally affixed ventricular restraint early after MI reduces infarct expansion, moderates regional stress distribution, improves BZ contractile function and, most importantly, limits long-term global LV remodeling in large-animal MI models [21, 58-61]. Although these studies have established the prevention of early infarct expansion as a potentially important therapeutic goal, it is unlikely that the surgical placement of restraining devices early after MI will gain widespread acceptance and application. As a result, there has been extensive experimental work to study the effect of injecting percutaneously deliverable biomaterials into the infarct to limit global LV

remodeling [24, 62-64]. While our results have demonstrated improvement in remodeling, the effect of these materials on regional myocardial stress distribution and BZ contractile function has not been fully established. In this study, the approach was to employ a state-of-the art MRI-based finite element (FE) model that employs subject-specific LV geometry to assess the effect of early post-MI infarct delivery of a novel shear-thinning biomaterial system on regional post-MI contractile function and regional myocardial stress distribution at 8 weeks after MI in an ovine infarct model.

5.2   Materials and Method

5.2.1 Infarct model

The data examined in the current study were collected in the course of a preceding study by Rodell et al [24] wherein protocols complied with the University of Pennsylvania's Institutional Animal Care and Use Committee and animal care was in agreement with the National Institute of Health's guidelines for the care and use of laboratory animals (NIH Publication 85-23, revised 1996). In brief, Dorset sheep (adult male, 45kg) underwent left thoracotomy to expose the heart. Posterolateral infarction was produced by suture ligation of selective obtuse marginal branches, resulting in infarcts comprising approximately 20% of the left ventricle. Sixteen injections (0.3 mL each) of saline (MI control, n=6) or dual-crosslinking hydrogels (DC treatment, n=6) were performed within the infarcted region. DC hydrogels were prepared by separate modification of hyaluronic acid (HA) by both adamantane and thiols (Ad-HA-SH) or β-cyclodextrin and

50

methacrylates (CD-MeHA), with injectable hydrogels formed by their combination at a pH of 5 under sterile conditions as previously reported [24, 65].

5.2.2 *Magnetic resonance (MR) imaging and analysis*

At 8 weeks post-infarction, MR image acquisition was performed (3T MAGNETOM Trio; Siemens; Malvern, PA) under maintained anesthesia (1-2% isoflurane) with cardiac gating using LV placement of a pressure transducer (Millar Instruments; Houston, TX), with magnetic tagging triggered at onset of systole. Recorded pressures were later used to determine loading in the model. 3D SPAMM was performed to enable generation of animal-specific LV geometry and determination of corresponding tissue displacement fields (field of view = 260 mm × 260 mm, acquisition matrix = 256 × 128, pixel size = 1.015 mm × 1.015 mm, repetition time = 34.44 ms, tag spacing = 6 mm, bandwidth = 331 Hz/pixel, slice thickness = 2 mm, averages = 4) [66]. Late-gadolinium enhanced (LGE) images were acquired 15 minutes following bolus administration of 0.1 mmol/kg gadobenate dimeglumine (MultiHance; Bracco Diagnostics; Cranbury, NJ) to confirm designation of the infarct region (field of view = 218 x 350 mm, acquisition matrix = 256 x 160, pixel size = 1.37x1.37 mm, repetition time = 5.50 ms, echo time = 2.42 ms, BW 244 Hz/pixel, slice thickness = 4 mm, averages = 2).

Both epicardial and endocardial contours of the LV were generated (ImageJ; Bethesda, MD) from 3D SPAMM images at onset of systole to enable strain calculation by application of optical flow methods [66]. Contours were similarly generated at early diastole to generate the animal-specific reference geometry, including isolation of the endocardial and epicardial segments of the infarct region,

which was aided by synchronization with LGE images. Endocardial contours were used to determine the end-systolic (ESV) and end-diastolic (EDV) LV volumes.

5.2.3 Finite Element modeling

Finite element models were created based on each animal-specific LV geometry at early diastole. This configuration was chosen because the stress in the LV is at a minimum. The geometry of LV wall was based on experimental measurements from MRI. The infarct region was defined base on the LGE imaging discussed previously. The BZ region was approximated as a 20-degree sector which transitions from the infarct region to the remote region [67] (Figure 18).

Each animal-specific LV FE mesh (MI, n=6; DC, n=6) was produced using tri-linear hexahedral brick elements, which were fit to 3D geometric surfaces that were generated from the endocardial and epicardial contours (TrueGrid; XYZ Scientific, Inc., Livermore, CA). The myofiber orientation in the remote, BZ, and infarct regions were assigned from epicardium to endocardium using the angles of -27 degrees to 88 degrees [48], -20 degree to 70 degree [68], and -5 degree to 26 degree [48] respectively. For the DC cases, the infarct region was modified to include a pattern of hydrogel injections embedded within the wall (Figure 19(b)). The pattern and volume were approximated from MR images of a representative in-vivo injection (Figure 19(a)). It should be noted that the MRI reconstruction, shown in Figure 19(a), was only conducted on a single animal. Therefore, the injection pattern in each of the six DC cases was approximated from this distribution. Since each injection was 0.3 ml, the total amount of volume added to

the infarct region was 4.8 ml. The endocardial wall of each MI and DC LV model was loaded with a pressure boundary condition, based on the experimentally measured values from the pressure transducer. Boundary conditions were implemented at the base of the LV to fully constrain displacement on the epicardial-basal edge, while allowing the remaining basal nodes to move in the circumferential-radial plane.

5.3   Material response

The material response of the passive myocardium was represented in Eq1. The diastolic animal-specific material parameters, C in the remote region and C_I in the infarct region were optimized to match the corresponding EDV from MRI in each animal. Based on a previous study, the passive material parameters in the exponential function were assigned differently in the remote region (b_f, b_t, b_{fs}) and the infarct region (b_f_I, b_t_I, b_{fs}_I) for the MI case and DC case (MI: b_f=37.67, b_t=17.39, b_{fs}=23.12, b_f_I=22.67, b_t_I=19, b_{fs}_I=18.12, DC: b_f=22.84, b_t=3.46, b_{fs}=12, b_f_I=15.28, b_t_I=8.32, b_{fs}_I=25.27) [48]. Note that the passive material parameters chosen in the BZ region were the same as the remote regions at 8 weeks post-infarction. The bulk modulus was assigned as κ = 1.0 MPa.

The material response of the hydrogel injections was represented in Eq 3. The material parameters for Young's modulus (E) were assigned based on the experimental measurements of the DC hydrogels at 8 weeks (E=4.5 kPa,

determined in previous study [17]), while the Poison ratio (v) was assigned a value of 0.499 (due to near incompressibility).

Systolic stress was modeled using Eq 4. The systolic material parameter associated with the maximum isometric tension, within the remote (T_{max_R}), and BZ (T_{max_B}) region, was calculated using numerical optimization. The parameter in the infarct region (T_{max_I}) was assigned to be zero, which was confirmed in previous work [69]. The initial search range in the optimization was set between 50 kPa and 400 kPa for T_{max_R} and between 10 kPa and 300 kPa for T_{max_B}, while $T_{\mathrm{max}\_I} = 0$. A cross-fiber in-plane stress component equivalent to 40% of the fiber component was added based on previous studies of LV contraction [34].

5.4 Optimization

Each FE simulation was conducted in two phases, where the first phase represented passive diastolic filling and the second phase represented active systolic contraction to end-systole (LS-DYNA, Livermore Software Technology Corporation, Livermore, CA). The genetic algorithm (GA) was used to minimize the objective function, which was taken to be the sum of the squared error (SE) between the experimentally measured systolic strain data from MRI and FE predicted results, and was defined as

$$SE = \sum_{n=1}^{N} \sum_{i,j=1,2,3} w_n \left(E_{ij,n} - \bar{E}_{ij,n}\right)^2 + \left(\frac{V-\bar{V}}{\bar{V}}\right)^2 \qquad \text{(Eq 7)}$$

where n is the strain point within the myocardium, N is the total number of strain points, $E_{ij,n}$ and V are the FE predicted end-systolic strain and LV cavity volume, respectively. The over bar variables represent in-vivo measured values. Since there were fewer strain points measured in the BZ region compared to the remote region, the weight for the SE in the BZ was set to 3 while the rest were set to 1.

5.5   Statistical analysis

Data is presented as mean ± standard error (SEM) of the mean. For T_{max} and ES fiber stress, comparison between groups (MI, DC) was performed by two-tailed student's t-test with significant determined at p < 0.05. For the MI model and DC model, statistical significance in different regions was determined by one-way ANOVA. Bonferroni test was used to account for multiple comparisons procedures with α=0.05.

5.6   Results

The average diastolic animal-specific material parameters, C in the remote region and C_I in the infarct region, were determined such that the model EDV matched the corresponding EDV from MRI. The values were found to be C=0.15±0.06 kPa and C_I=9.43±4.45 kPa for the MI cases and C=0.893±0.24 and C_I=23.67±4.55 for the DC cases, respectively. The contractility parameter T_{max} was determined from optimization of all animal-specific models. For the MI case, the parameter T_{max_R} =205.29±40.98 kPa and T_{max_B} =49.31±15.56 kPa. This

represents a 76% reduction in contractile force in the BZ of the untreated MI controls, relative to the remote region. For the DC case, T_{max_R}=163.66±25.23 kPa and T_{max_B}=122.13±26.82 kPa. This represents only a 25% reduction in contractile force in the BZ of treated animals, relative to the remote region. In terms of the fit achieved during the optimization, the average SE value for the MI case was 25.9±2.3 and for the DC case was 22.8±3.1.

In the remote region, the difference in contractile function between the DC and MI case was not associated with any statistical significance (p=0.407) (Figure 20a). In contrast, the contractility in the BZ region predicted in the DC case was higher and significantly different from the MI case (p*=0.0408) (Figure 20a). Additionally, in the MI case, the contractile function was significantly different between the remote region and BZ region (p*=0.005) (Figure 20a). However, the tissue contractile function in the DC case was similar when comparing between the remote region and BZ region, i.e., no statistical significance (p=0.286) (Figure 20a). These results indicate that the BZ tissue in the DC case has higher contractility compared to the MI case.

The average wall thickness within the infarct region at end-diastole for the MI and DC cases were 0.5±0.02 cm and 1.05±0.06 cm, respectively. In the BZ region, the average wall thickness was measured to be 0.64±0.01 cm and 0.86±0.04 cm for MI and DC cases, respectively. In the remote region, the average wall thickness in the MI case was 0.975±0.05 cm while in the DC case was 0.985±0.05 cm. This indicated that the DC hydrogel treatment reduced wall

thinning at 8 weeks post-infarction and a significant difference was observed between the DC and MI cases [24].

The average ES fiber stress in the infarct region of the DC case was significantly reduced by 40% relative to the MI case (MI: 47.28±6.11 kPa, DC: 28.52±3.83 kPa; p*=0.0264). The averages ES fiber stress of the DC case in the BZ region was also significantly reduced by 33% relative to the MI case (MI: 28.96±1.94 kPa, DC: 19.36±1.71 kPa; p*=0.0041). In the remote region, the ES fiber stress shows a significant reduction of 34% compared to the MI case (MI: 22.08±1.46 kPa, DC: 14.59±2.07 kPa; p*=0.0144) (Figure 20b). The end-systolic fiber stress distribution in different regions of the mid-ventricle wall are shown for a representative DC hydrogel injection case (Figure 21a) and a representative control MI case (Figure 21c). Figures 20b and 20d indicate the different material regions for evaluating the fiber stress distribution, and also show the differences in wall thickness at end-systole.

5.7   Discussion

Despite the established efficacy and widespread availability of reperfusion therapy, myocardial infarction resulting from coronary artery disease and subsequent adverse LV remodeling remains a leading cause of heart failure [70]. In the majority of acute MI patients, the LV function is initially preserved and only after months or years do symptoms of heart failure develop. The severity of the LV response to MI (i.e. LV remodeling) is determined by the size, location and transmurality of the infarct. Initially this response is largely mechanical, but with

time these physical phenomena initiate a complex cascade of progressive maladaptive biologic sequelae that permanently compromise the contractile function of the perfused myocardium outside of the infarcted region [17].

Infarct expansion (i.e. stretching) early after MI has long been recognized as a clinical risk factor for adverse LV remodeling and the development of heart failure symptoms. It has been demonstrated that early infarct expansion is associated with increased mechanical stress in the infarct and adjacent BZ region, which results in progressive loss of contractile function in perfused myocardium adjacent to the infarct. It has also been shown that this dysfunctional BZ becomes more hypocontractile and progresses to involve additional perfused myocardium as remodeling continues and heart failure develops [17].

In an extensive series of preclinical large animal studies, it was demonstrated that infarct restraint with mesh wrapping devices in the early post MI period normalizes regional LV stress, preserves BZ contractility, and limits global LV remodeling [22, 58-61]. This work strongly supports the idea that the prevention of infarct expansion is an important therapeutic goal intended to limit MI-induced LV remodeling. However, the use of external restraint devices in the form of mesh jackets and patches is never likely to achieve widespread clinical application because of the invasive surgical procedures that would be required in the early post-MI period to place them. Given this clinical reality, researchers have begun to explore and develop the use of hydrogel biomaterials to modify infarct material characteristics to limit or prevent progressive infarct expansion [24, 62-64]. The use of such materials holds the potential for percutaneous, catheter-based

58

approaches for beneficially altering the post-MI LV remodeling process. The novel shear-thinning biomaterial system tested in this study is an emerging candidate for translation into patents because it can be administered through long, narrow catheters but at the same time can be engineered to the appropriate stiffness for optimally limiting infarct expansion [65].

The efficacy of this biomaterial system on post MI LV remodeling has been previously reported [24]. However, its effect on regional myocardial stress distribution and BZ contractile function had not yet been assessed. To better elucidate the biomechanical mechanism by which this hydrogel system affects the remodeling process, the current study employed a state-of-the-art MRI-based finite element model that employs subject-specific LV geometry to assess the effect on regional post-MI contractile function and regional myocardial stress distribution at 8 weeks after MI in an ovine infarct model.

Utilizing this approach, it was found that contractility in the BZ of animals treated with hydrogel injection was significantly higher than untreated controls, indicating that function is better retained due to treatment. This result shows strong agreement with purely MRI-based studies, which found that ES principal strains were higher in animals treated with hydrogel injections (implying stronger contraction) [48]. It was also found that the passive stiffness of the treated infarct region was much greater than the untreated control. Additionally, the wall thickness in the infarct and BZ regions were significantly higher in the treated animals. Both of these factors are likely contributors to the fact that end-systolic fiber stress was greatly reduced in the BZ of treated animals.

Treatment with hydrogel injection significantly improved BZ function and reduced LV remodeling, via altered MI properties. These changes are linked to a reduction in the ES fiber stress experienced in the BZ myocardium surrounding the infarct. The current results, in conjunction with those reported previously, imply that the novel shear-thinning hydrogel system used in this study should be a viable therapy for mitigating adverse LV remodeling after MI.
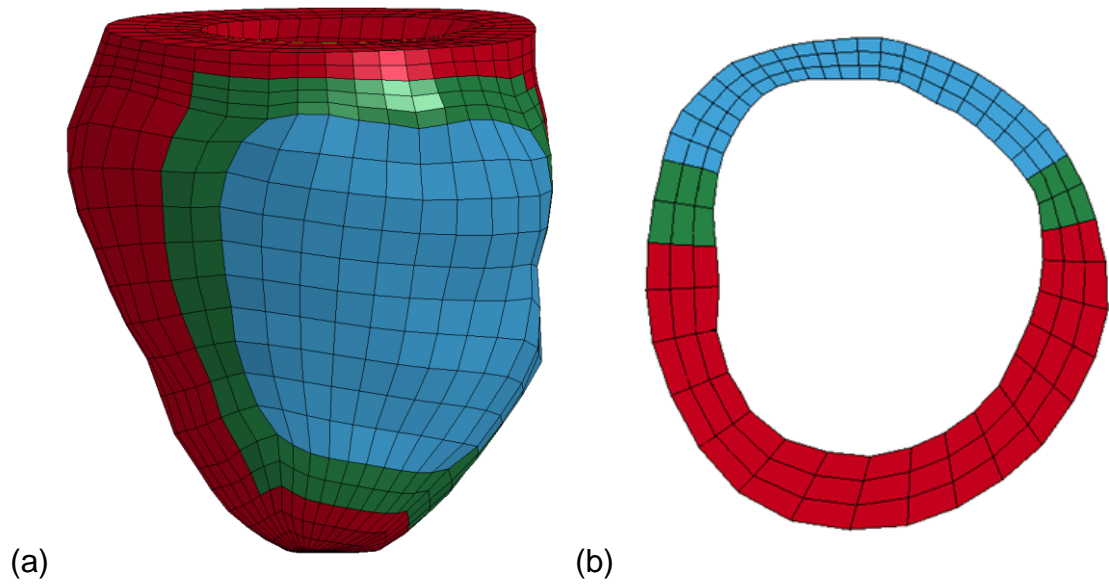
Figure 18 (a) Animal-specific FE model. The red elements represent the remote region, green elements are BZ region, and blue elements are the infarct region. (b) Short axis cross-section view of the animal-specific FE model near mid-ventricle.
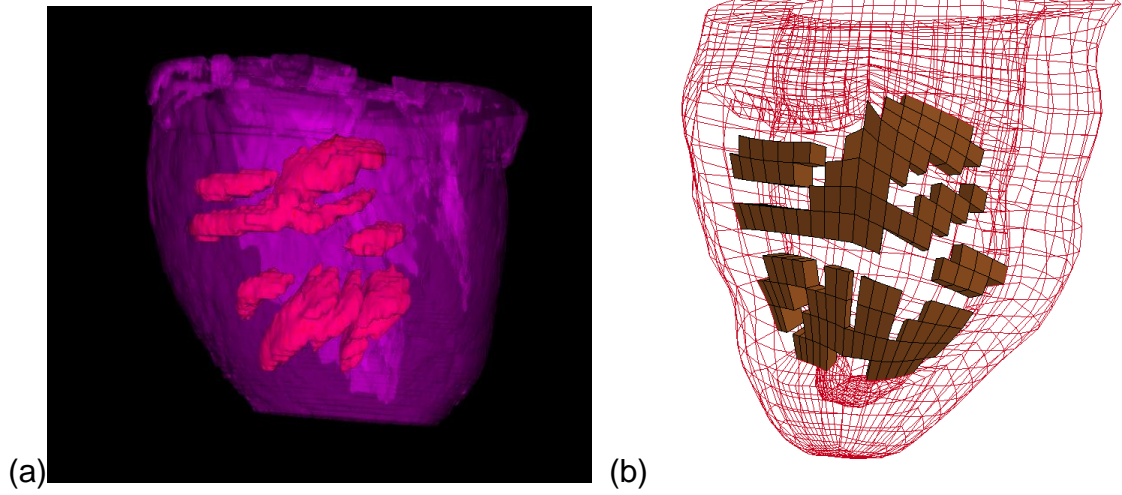
Figure 19 (a) MRI reconstruction of retained DC hydrogel (red) within the infarct region (purple) in vivo [24]. (b) DC FE model with approximated hydrogel injection pattern (brown) within the infarct.
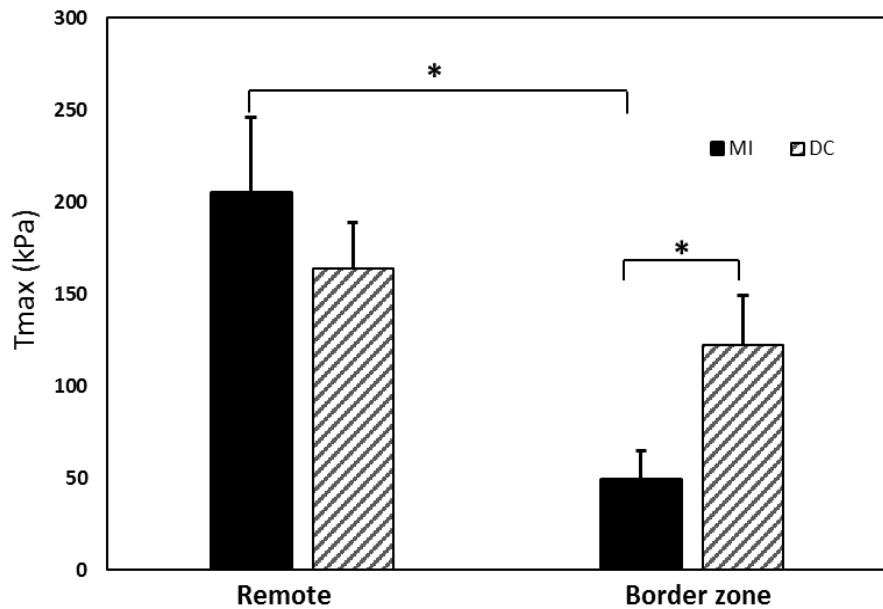
(a)
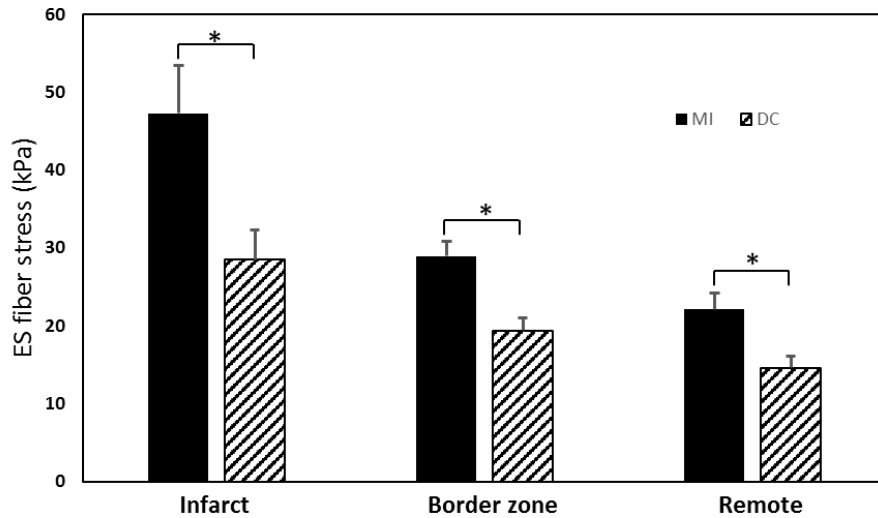
(b)

Figure 20 (a) Comparison of T_max distribution between MI case and DC case in remote region and BZ region, respectively. (b) Comparison of end-systolic (ES) fiber stress between MI case and DC case in the infarct, BZ, and remote regions, respectively.
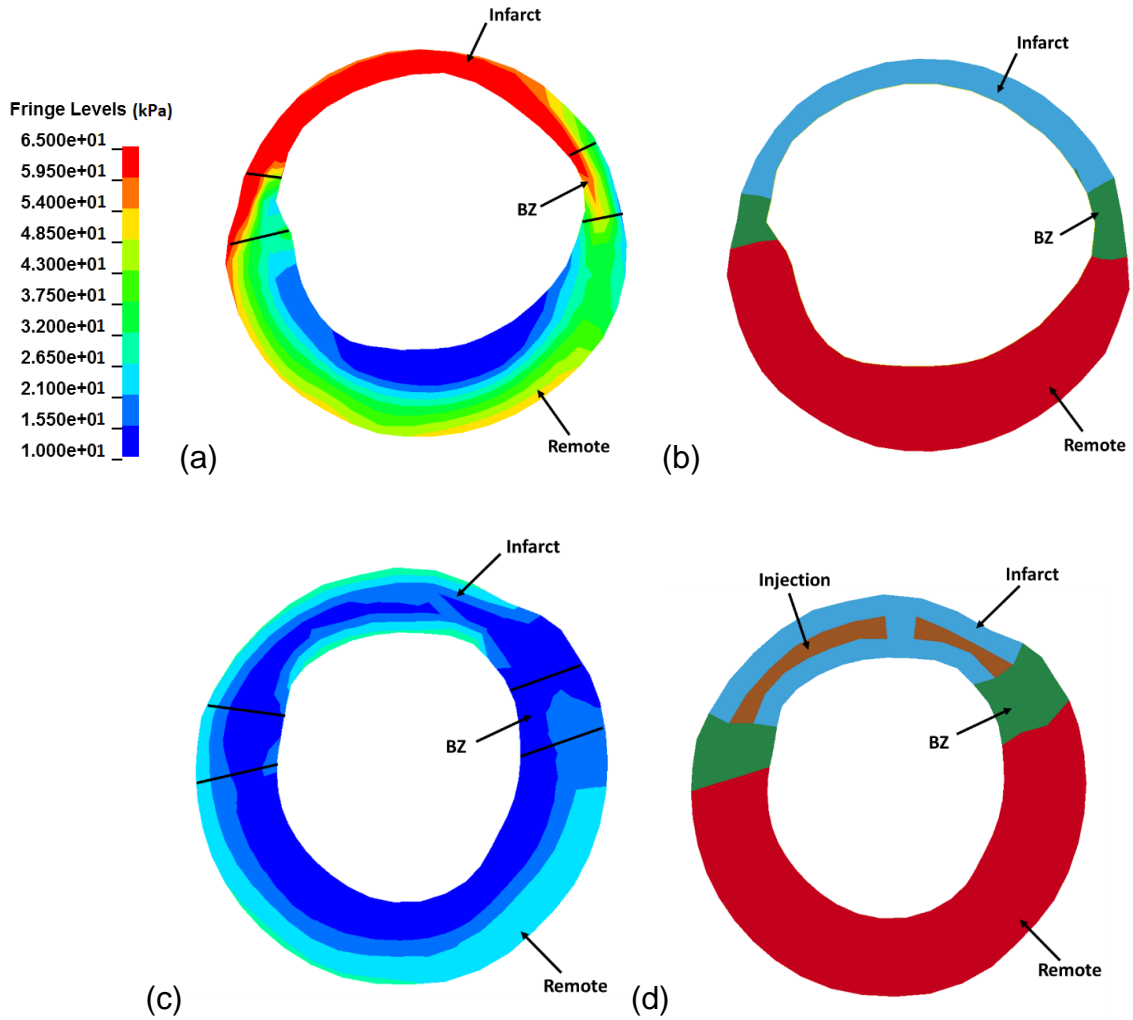
Figure 21 (a) End-systolic fiber stress distribution in cross section view of an animal-specific MI FE model near mid-ventricle. (b) Cross section view of the MI FE model at end-systole in same location. (c) End-systolic fiber stress distribution in cross section.

Chapter 6   **Conclusion**

To sum up this dissertation, Chapter 3 utilized MRI data and computational modeling to estimate the in vivo contractile forces generated in three different transmural regions of healthy pig ventricles. The primary conclusion is that a FE model with non-uniform contractility distribution is more representative of the deformation that occurs in-vivo. Chapter 4 evaluated the sensitivity effect of hydrogel stiffness for treating myocardial infarction compared to control injection case. This study is a continuation of a previous study [24], in which this treatment was beneficial to prevent dilation of the left ventricle over the time of the remodeling process. The current study employed a combination of experimental data and FE modeling to correlate how injection stiffness and volume influence myocardial wall stress and wall thickness. The conclusion was that by tuning the stiffness of hydrogel, greater reductions in fiber stress can be achieved, but these improvements begin to taper after a stiffness of 50 kPa. Chapter 5 expanded on the baseline work conducted in Chapter 3 by assessing the contractility in MI control and DC hydrogel injection treated animals. In this study, contractility in the BZ of animals treated with hydrogel injection was significantly higher than untreated animals. Additionally, the wall thickness in the infarct and BZ were found to be significantly higher in the treated animals. These results imply that injectable hydrogels could be a viable therapy for maintaining LV function post myocardial infarction

.

References

1.   Mozaffarian, D., et al., *Executive summary: Heart Disease and Stroke Statistics-2016 update: A report from the American Heart Association.* Circulation, 2016. **133**(4): p. 447.
2.   Guccione, J.M., L.K. Waldman, and A.D. McCulloch, *Mechanics of active contraction in cardiac muscle: Part II--Cylindrical models of the systolic left ventricle.* J Biomech Eng, 1993. **115**(1): p. 82-90.
3.   Lou, Q., et al., *Transmural heterogeneity and remodeling of ventricular excitation-contraction coupling in human heart failure.* Circulation, 2011. **123**(17): p. 1881-1890.
4.   Campbell, S.G., et al., *Altered ventricular torsion and transmural patterns of myocyte relaxation precede heart failure in aging F344 rats.* American Journal of Physiology-Heart and Circulatory Physiology, 2013. **305**(5): p. H676-H686.
5.   Stelzer, J.E., et al., *Transmural variation in myosin heavy chain isoform expression modulates the timing of myocardial force generation in porcine left ventricle.* J Physiol, 2008. **586**(Pt 21): p. 5203-14.
6.   van der Velden, J., et al., *Isometric tension development and its calcium sensitivity in skinned myocyte-sized preparations from different regions of the human heart.* Cardiovasc Res, 1999. **42**(3): p. 706-19.
7.   Haynes, P., et al., *Transmural heterogeneity of cellular level power output is reduced in human heart failure.* J Mol Cell Cardiol, 2014. **72**: p. 1-8.
8.   Streeter, D.D., Jr., et al., *Fiber orientation in the canine left ventricle during diastole and systole.* Circ Res, 1969. **24**(3): p. 339-47.
9.   Carew, T.E. and J.W. Covell, *Fiber orientation in hypertrophied canine left ventricle.* Am J Physiol, 1979. **236**(3): p. H487-93.
10.   Holmes, J.W., T.K. Borg, and J.W. Covell, *Structure and mechanics of healing myocardial infarcts.* Annu Rev Biomed Eng, 2005. **7**: p. 223-53.
11.   Hutchins, G.M. and B.H. Bulkley, *Infarct expansion versus extension: two different complications of acute myocardial infarction.* The American journal of cardiology, 1978. **41**(7): p. 1127-1132.
12.   Humphrey, J.D. and F.C. Yin, *On constitutive relations and finite deformations of passive cardiac tissue: I. A pseudostrain-energy function.* J Biomech Eng, 1987. **109**(4): p. 298-304.
13.   Eaton, L.W., et al., *Regional cardiac dilatation after acute myocardial infarction: recognition by two-dimensional echocardiography.* N Engl J Med, 1979. **300**(2): p. 57-62.
14.   Erlebacher, J.A., et al., *Early dilation of the infarcted segment in acute transmural myocardial infarction: role of infarct expansion in acute left ventricular enlargement.* J Am Coll Cardiol, 1984. **4**(2): p. 201-8.
15.   Weisman, H.F. and B. Healy, *Myocardial infarct expansion, infarct extension, and reinfarction: pathophysiologic concepts.* Prog Cardiovasc Dis, 1987. **30**(2): p. 73-110.

16.   Epstein, F.H., et al., *MR tagging early after myocardial infarction in mice demonstrates contractile dysfunction in adjacent and remote regions.* Magn Reson Med, 2002. **48**(2): p. 399-403.

17.   Jackson, B.M., et al., *Extension of borderzone myocardium in postinfarction dilated cardiomyopathy.* J Am Coll Cardiol, 2002. **40**(6): p. 1160-7; discussion 1168-71.

18.   Jackson, B.M., et al., *Border zone geometry increases wall stress after myocardial infarction: contrast echocardiographic assessment.* Am J Physiol Heart Circ Physiol, 2003. **284**(2): p. H475-9.

19.   Kramer, C.M., et al., *Regional differences in function within noninfarcted myocardium during left ventricular remodeling.* Circulation, 1993. **88**(3): p. 1279-88.

20.   Lima, J.A., et al., *Impaired thickening of nonischemic myocardium during acute regional ischemia in the dog.* Circulation, 1985. **71**(5): p. 1048-59.

21.   Pilla, J.J., et al., *Early postinfarction ventricular restraint improves borderzone wall thickening dynamics during remodeling.* Ann Thorac Surg, 2005. **80**(6): p. 2257-62.

22.   Wilson, E.M., et al., *Region- and type-specific induction of matrix metalloproteinases in post-myocardial infarction remodeling.* Circulation, 2003. **107**(22): p. 2857-63.

23.   Goldthwaite Jr, C.A., *Mending a broken heart: Stem cells and cardiac repair.* NIH report, 2007.

24.   Rodell, C.B., et al., *Injectable shear-thinning hydrogels for minimally invasive delivery to infarcted myocardium to limit left ventricular remodeling.* Circulation: Cardiovascular Interventions, 2016. **9**(10): p. e004058.

25.   Wenk, J.F., et al., *A method for automatically optimizing medical devices for treating heart failure: designing polymeric injection patterns.* J Biomech Eng, 2009. **131**(12): p. 121011.

26.   Tözeren, A., *Continuum rheology of muscle contraction and its application to cardiac contractility.* Biophysical journal, 1985. **47**(3): p. 303.

27.   Campbell, S.G., et al., *Altered ventricular torsion and transmural patterns of myocyte relaxation precede heart failure in aging F344 rats.* Am J Physiol Heart Circ Physiol, 2013. **305**(5): p. H676-86.

28.   Lou, Q., et al., *Transmural heterogeneity and remodeling of ventricular excitation-contraction coupling in human heart failure.* Circulation, 2011. **123**(17): p. 1881-90.

29.   Wang, V.Y., et al., *Modelling passive diastolic mechanics with quantitative MRI of cardiac structure and function.* Med Image Anal, 2009. **13**(5): p. 773-84.

30.   Xi, J., et al., *The estimation of patient-specific cardiac diastolic functions from clinical measurements.* Med Image Anal, 2013. **17**(2): p. 133-46.

31.   Mojsejenko, D., et al., *Estimating passive mechanical properties in a myocardial infarction using MRI and finite element simulations.* Biomech Model Mechanobiol, 2015. **14**(3): p. 633-647.

32. McGarvey, J.R., et al., *Temporal Changes in Infarct Material Properties: An In Vivo Assessment using MRI and Finite Element Simulations.* Annals of Thoracic Surgery, 2015. **100**(2): p. 582-589.

33. Sun, K., et al., *A computationally efficient formal optimization of regional myocardial contractility in a sheep with left ventricular aneurysm.* J Biomech Eng, 2009. **131**(11): p. 111001.

34. Walker, J.C., et al., *MRI-based finite-element analysis of left ventricular aneurysm.* Am J Physiol Heart Circ Physiol, 2005. **289**(2): p. H692-700.

35. Wenk, J.F., et al., *Regional Left Ventricular Myocardial Contractility and Stress in a Finite Element Model of Posterobasal Myocardial Infarction.* Journal of Biomechanical Engineering-Transactions of the Asme, 2011. **133**(4).

36. Xu, C., et al., *Deformation analysis of 3D tagged cardiac images using an optical flow method.* J Cardiovasc Magn Reson, 2010. **12**: p. 19.

37. McGarvey, J.R., et al., *Temporal changes in infarct material properties: an in vivo assessment using magnetic resonance imaging and finite element simulations.* The Annals of thoracic surgery, 2015. **100**(2): p. 582-589.

38. Wenk, J.F., et al., *First evidence of depressed contractility in the border zone of a human myocardial infarction.* Ann Thorac Surg, 2012. **93**(4): p. 1188-93.

39. Wenk, J.F., et al., *Regional left ventricular myocardial contractility and stress in a finite element model of posterobasal myocardial infarction.* J Biomech Eng, 2011. **133**(4): p. 044501.

40. Zhang, X., et al., *Numerical evaluation of myofiber orientation and transmural contractile strength on left ventricular function.* J Biomech Eng, 2015. **137**(4).

41. Guccione, J.M., K.D. Costa, and A.D. McCulloch, *Finite element stress analysis of left ventricular mechanics in the beating dog heart.* J Biomech, 1995. **28**(10): p. 1167-77.

42. Omens, J.H., K.D. May, and A.D. McCULLOCH, *Transmural distribution of three-dimensional strain in the isolated arrested canine left ventricle.* American Journal of Physiology-Heart and Circulatory Physiology, 1991. **261**(3): p. H918-H928.

43. Nash, M.P. and P.J. Hunter, *Computational mechanics of the heart.* Journal of elasticity and the physical science of solids, 2000. **61**(1-3): p. 113-141.

44. Rodriguez, E.K., et al., *Effect of residual stress on transmural sarcomere length distributions in rat left ventricle.* Am J Physiol, 1993. **264**(4 Pt 2): p. H1048-56.

45. Ifkovits, J.L., et al., *Injectable hydrogel properties influence infarct expansion and extent of postinfarction left ventricular remodeling in an ovine model.* Proceedings of the National Academy of Sciences, 2010. **107**(25): p. 11507-11512.

46. Morita, M., et al., *Modification of infarct material properties limits adverse ventricular remodeling.* Ann Thorac Surg, 2011. **92**(2): p. 617-24.

47. Tous, E., et al., *Injectable acellular hydrogels for cardiac repair.* Journal of cardiovascular translational research, 2011. **4**(5): p. 528-542.

48. Dorsey, S.M., et al., *MRI evaluation of injectable hyaluronic acid-based hydrogel therapy to limit ventricular remodeling after myocardial infarction.* Biomaterials, 2015. **69**: p. 65-75.

49. Rodell, C.B., et al., *Shear-Thinning Supramolecular Hydrogels with Secondary Autonomous Covalent Crosslinking to Modulate Viscoelastic Properties In Vivo.* Adv Funct Mater, 2015. **25**(4): p. 636-644.

50. Ryan, L.P., et al., *Dermal filler injection: a novel approach for limiting infarct expansion.* The Annals of thoracic surgery, 2009. **87**(1): p. 148-155.

51. Kichula, E.T., et al., *Experimental and computational investigation of altered mechanical properties in myocardium after hydrogel injection.* Annals of biomedical engineering, 2014. **42**(7): p. 1546-1556.

52. Lee, L.C., et al., *Bioinjection treatment: effects of post-injection residual stress on left ventricular wall stress.* J Biomech, 2014. **47**(12): p. 3115-9.

53. Wise, P., et al., *Excessive volume of hydrogel injectates may compromise the efficacy for the treatment of acute myocardial infarction.* Int J Numer Method Biomed Eng, 2016. **32**(12).

54. Plotkin, M., et al., *The effect of matrix stiffness of injectable hydrogels on the preservation of cardiac function after a heart attack.* Biomaterials, 2014. **35**(5): p. 1429-1438.

55. Landa, N., et al., *Effect of injectable alginate implant on cardiac remodeling and function after recent and old infarcts in rat.* Circulation, 2008. **117**(11): p. 1388-1396.

56. Mukherjee, R., et al., *Targeted myocardial microinjections of a biocomposite material reduces infarct expansion in pigs.* The Annals of Thoracic Surgery, 2008. **86**(4): p. 1268-1276.

57. Rane, A.A. and K.L. Christman, *Biomaterials for the treatment of myocardial infarction: a 5-year update.* Journal of the American College of Cardiology, 2011. **58**(25): p. 2615-2629.

58. Blom, A.S., et al., *Ventricular restraint prevents infarct expansion and improves borderzone function after myocardial infarction: a study using magnetic resonance imaging, three-dimensional surface modeling, and myocardial tagging.* Ann Thorac Surg, 2007. **84**(6): p. 2004-10.

59. Enomoto, Y., et al., *Early ventricular restraint after myocardial infarction: extent of the wrap determines the outcome of remodeling.* Ann Thorac Surg, 2005. **79**(3): p. 881-7; discussion 881-7.

60. Kelley, S.T., et al., *Restraining infarct expansion preserves left ventricular geometry and function after acute anteroapical infarction.* Circulation, 1999. **99**(1): p. 135-42.

61. Moainie, S.L., et al., *Infarct restraint attenuates remodeling and reduces chronic ischemic mitral regurgitation after postero-lateral infarction.* Ann Thorac Surg, 2002. **74**(2): p. 444-9; discussion 449.

62. Ifkovits, J.L., et al., *Injectable hydrogel properties influence infarct expansion and extent of postinfarction left ventricular remodeling in an ovine model.* Proc Natl Acad Sci U S A, 2010. **107**(25): p. 11507-12.

63. Ryan, L.P., et al., *Dermal filler injection: a novel approach for limiting infarct expansion.* Ann Thorac Surg, 2009. **87**(1): p. 148-55.

64. Tous, E., et al., *Influence of injectable hyaluronic acid hydrogel degradation behavior on infarction-induced ventricular remodeling.* Biomacromolecules, 2011. **12**(11): p. 4127-35.

65. Rodell, C.B., et al., *Shear-Thinning Supramolecular Hydrogels with Secondary Autonomous Covalent Crosslinking to Modulate Viscoelastic Properties In Vivo.* Advanced Functional Materials, 2015. **25**(4): p. 636-644.

66. Xu, C., et al., *Deformation analysis of 3D tagged cardiac images using an optical flow method.* Journal of Cardiovascular Magnetic Resonance, 2010. **12**: p. 12-19.

67. Pilla, J.J., et al., *Regional myocardial three-dimensional principal strains during postinfarction remodeling.* The Annals of thoracic surgery, 2015. **99**(3): p. 770-778.

68. Wu, M.-T., et al., *Sequential changes of myocardial microstructure in patients postmyocardial infarction by diffusion-tensor cardiac MR correlation with left ventricular structure and function.* Circulation: Cardiovascular Imaging, 2009. **2**(1): p. 32-40.

69. Wenk, J.F., et al., *Regional left ventricular myocardial contractility and stress in a finite element model of posterobasal myocardial infarction.* Journal of biomechanical engineering, 2011. **133**(4): p. 044501.

70. Mozaffarian, D., et al., *Heart Disease and Stroke Statistics-2016 Update: A Report From the American Heart Association.* Circulation, 2016. **133**(4): p. e38-360.

VITA

Hua Wang was born in Dongying, Shandong, China. After completing her work at high school, in 2008, she entered China University of Mining and Technology, Jiangsu, China. After two years, she joined a 2+2 combined education program that was cosponsored by the University of Kentucky. She received the degree of Bachelor of Science both from University of Kentucky and China University of Mining and Technology in May 2012. Since 2012, she joined the Computational Biomechanics Laboratory, which is run by Dr. Jonathan Wenk to continue Master's degree and Ph.D.'s degree until 2017.

Publications:

1. **Wang, H**., Rodel, C.B., Zhang, X., Lee, M.E. Takebayashi, S., Takayama, T., Burdick, J.A., Gorman, J.H., Pilla, J.J., Gorman, R.C. and Wenk, J.F., 2016. Computational Investigation of Injectable Hydrogels Therapy to Limit Ventricular Remodeling after Myocardial Infarction. The Annals of Thoracic Surgery. (Under review)

2. **Wang, H**., Zhang, X., Dorsey, S.M., McGarvey, J.R., Campbell, K.S., Burdick, J.A.,Gorman, J.H., Pilla, J.J., Gorman, R.C. and Wenk, J.F., 2016. Computational Investigation of Transmural Differences in Left Ventricular Contractility. Journal of Biomechanical Engineering, 138(11), p.114501.

3. Rodell, C.B., Lee, M.E., **Wang, H**., Zellars, K.N., Perreault, P.E., Gorman, J.H., Wenk, J.F., Spinale, F.G., Gorman, R.C. and Burdick, J.A., 2016. Injectable

Hydrogels for Minimally Invasive Delivery to Limit Infarct Induced Left Ventricular Remodeling and Mitral Regurgitation.

4. Rodell, C.B., Lee, M.E., **Wang, H**., Takebayashi, S., Takayama, T., Kawamura, T., Arkles, J.S., Dusaj, N.N., Dorsey, S.M., Witschey, W.R. and Pilla, J.J., 2016. Injectable Shear-Thinning Hydrogels for Minimally Invasive Delivery to Infarcted Myocardium to Limit Left Ventricular Remodeling. Circulation: Cardiovascular Interventions, 9(10), p.e004058.

5. Dorsey, S. M., McGarvey, J. R., **Wang, H**., Nikou, A., Arama, L., Koomalsingh, K. J., Kondo, N., Gorman III, J. H., Pilla, J. J., Gorman, R. C., Wenk, J. F., and Burdick, J. A., 2015, "MRI Evaluation of Injectable Hyaluronic Acid Hydrogel Therapy to Limit Ventricular Remodeling after Myocardial Infarction," Biomaterials, 69, pp. 65-75.(PMCID: PMC4556569)

6. Kichula, E. T., **Wang, H**., Dorsey, S. M., Szczesny, S. E., Elliott, D. M., Burdick, J. A., and Wenk, J. F., 2014, "Experimental and Computational Investigation of Altered Mechanical Properties in Myocardium after Hydrogel Injection," Annals of Biomedical Engineering, 42(7), pp. 1546-1556. (PMCID: PMC4032381)

This dissertation was typed by Hua Wang